MASTER

Ray-optics analysis of switchable auto-stereoscopic lenticular-based 2D/3D displays

Sluijter, M.

Award date:
2005

Eindhoven University of Technology
Department of Physics
Group Elementary Processes in Gas discharges

Ray-Optics Analysis of Switchable Auto-Stereoscopic Lenticular-Based 2D/3D Displays

M. Sluijter

December, 2005

Report Number: EPG 05-15

Report of a graduation project.
Supervisors: Dr. Ir. W.L. IJzerman and Dr. D.K.G. de Boer
Professor: Prof. Dr. Ir. G.M.W. Kroesen.

Abstract

In this thesis, the concept of multi-view switchable auto-stereoscopic lenticular-based 2D/3D displays is discussed. With the introduction of a switchable lenticular, it is possible to switch between a 2D mode and a 3D mode. The 2D mode images normal content, whereas the 3D mode provides the viewer with a three-dimensional impression. The performance of the 2D mode and the 3D mode is investigated by examining two quality parameters: modulation depth and crosstalk. Modulation depth is a measure for the angular dependency of the total intensity distribution of the display. Crosstalk is a measure for the overlap of the view distributions. In order to improve the quality parameters, spherical lenticulars as well as a-spherical lenticulars are investigated analytically and numerically, by using the concept of ray tracing. Based on the obtained results, we can draw the following conclusions.

The 3D performance of a switchable 2D/3D lenticular based display in the 3D mode can be improved with the use of artificially introduced additional lens aberrations in a lenticular. The use of this concept can considerably decrease the modulation depth keeping the crosstalk at an acceptable level.
The modulation depth in the 2D mode can be substantially decreased by using the concept of birefringent lens plates with a perfect index match between the lens material and the lens plate. The concept of birefringent lens plates can be used without disturbing the 3D performance of a switchable 2D/3D display.

Contents

1

Introduction

By combining its unique multi-view 3D display technology with advanced computer graphics and image analysis techniques, Philips Research developed an innovative technique of creating autostereoscopic three-dimensional images. The technology brings a new level of excitement and realism to computer gaming, video entertainment and professional imaging applications. In the near future, three-dimensional imaging can be seen in for instance advertisement and mobile phone displays.
In 2004, Philips Research developed a technique for 3D displays that makes it possible to switch between 2D content, for normal monitor applications, and 3D content, generating three-dimensional images [1]. This thesis contributes to the research and development of this technique.

1.1 Autostereoscopic imaging

Human depth perception is supported by a range of visual cues. These cues are generally known as depth cues. Depth cues can be divided into two categories, namely physiological cues and psychological cues.
Psychological depth cues include among other things linear perspective, shading and shadowing, interposition and texture gradient. These are all depth cues which can be used in ordinary 2D pictures.
Two main physiological depth cues that create a vivid three-dimensional impression are binocular disparity and motion parallax. Binocular disparity is the difference in images projected on the left and right eye of the viewer. Motion parallax provides different views of a scene in response to movement of the viewer. These physiological depth cues cannot be included in normal 2D pictures.

Many people are familiar with the concept of three-dimensional imaging using additional appliances, like polarized glasses. When using polarized glasses, distinct images are projected to each eye of the viewer, creating binocular disparity. One pair of distinct images is called a stereo pair.
Another option to create stereo pairs is by imaging different images towards different viewing angles. This method is called autostereoscopic imaging. Each

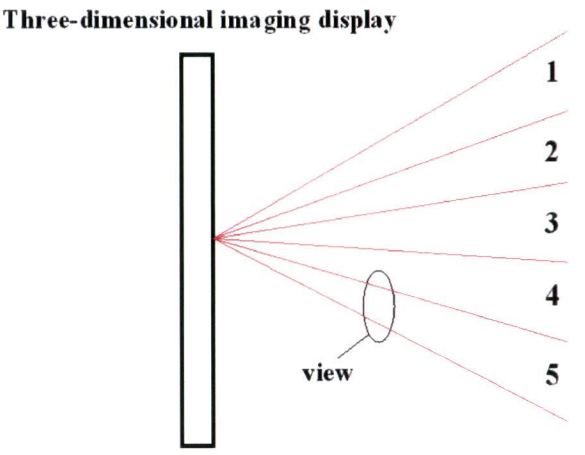

Figure 1.1: 3D display imaging 5 different views to 5 different viewing angles.

individual image is called a view. Views can be generated using a multi-view three-dimensional imaging display. The principle is shown in figure 1.1.
There are three main methods of autostereoscopic imaging, which differ in the way the views are separated for presentation to each eye. Using diffraction, refraction and occlusion, respectively, these are holographic, lenticular sheet and barrier strip techniques. Lenticular sheet and barrier strip techniques share many characteristics and are known as selector screen methods [2].

1.1.1 Parallax barrier

A parallax barrier consists of an array of fine vertical slits in an otherwise opaque barrier. Such a barrier can be placed a slight distance in front of a display, for example a liquid crystal display (LCD), see figure 1.2. According to the situation in figure 1.2, the pixels indicated by 'R' are the pixels that project an image in the right eye of the viewer. The pixels indicted by 'L' project an image on the viewer's left eye. The barrier ensures that the strips from each image will be visible only from the proper viewing direction so that each of the viewer's eyes is provided with a different image. The main disadvantage to the parallax barrier technique is that the image is often dim since so much light is blocked by the barrier.

The viewer depicted in figure 1.2 is correctly positioned to see an orthoscopic (normal) image. If the viewer moves to the side, the image seen by the left eye would be the one intended for the right eye and vice versa. In this case, depth relationships are reversed. Then, the viewer sees a pseudoscopic image. A normal image is obtained again if the viewer moves even further to the side.

1.1.2 Lenticular sheet

A lenticular sheet consists of an array of cylindrical lenses. This lenticular sheet is placed in front of an LCD (see figure 1.3). The sheet is designed in such a way,

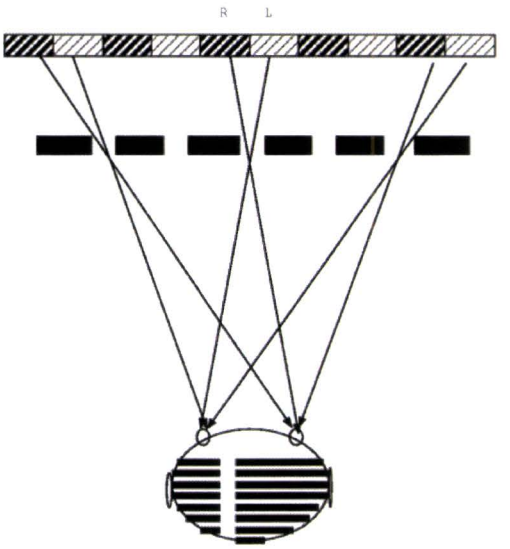

Figure 1.2: A parallax barrier uses occlusion to create views.

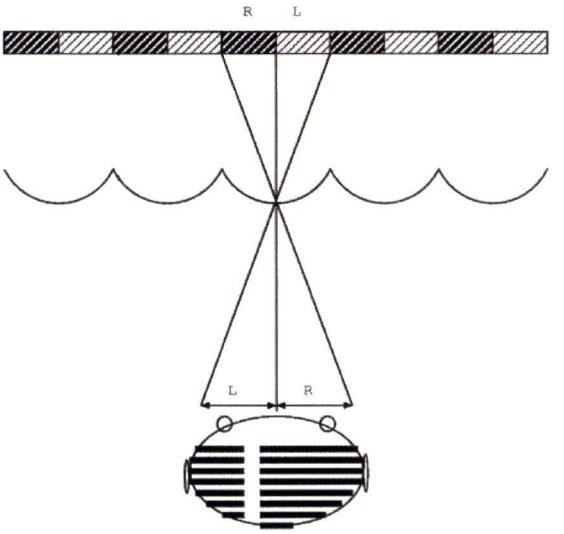

Figure 1.3: A lenticular sheet uses refraction to create views.

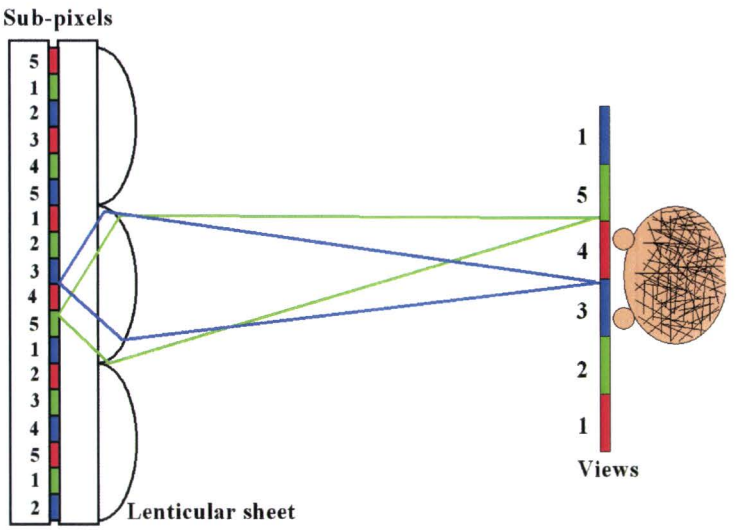

Figure 1.4: A multi-view lenticular based 3D display.

that the images of the 'R' and 'L' pixels are refracted to the right and left eye respectively. As a result, a stereo pair is formed. Lenticular displays have one significant advantage over barrier methods. Image brightness is superior since the lenticular sheet uses refraction rather than occlusion. This is an important argument to develop lenticular based displays rather than barrier strip displays.

1.2 Switchable 2D/3D displays based on liquid crystal lenses

Figure 1.4 shows a 5 views lenticular based 3D display. The sub-pixels of the display are numbered, each representing one of the 5 views. The sub-pixels are imaged by the lenses towards the viewer. The collection of sub-pixels numbered by 4, for example, is imaged in one particular area at the viewing distance, indicated by 4. The resulting image is one of the 5 views.
The production of a 3D display using a normal 2D display always involves a loss of resolution. This is simply because a 3D display containing N views uses sets of N sub-pixels to generate the views (see figure 1.4). Hence, the resolution of a 3D display is N times lower than the resolution of a normal 2D display.
If the lenticular is vertically oriented with respect to the display, the resolution loss is in the horizontal direction only. This is shown in the left part of figure 1.5. It shows a 9 views 3D display having a vertically aligned lenticular. In this example, all the bright red pixels contribute to the formation of 1 of the 9 views. Apparently, the viewer sees only 1 out of 9 sub-pixels when watching 1 view. In addition, the loss of information is in horizontal direction, since the sub-pixels corresponding to one view are all placed in successive columns.
If the lenticular of a 3D display is placed under a slant angle, the resolution loss

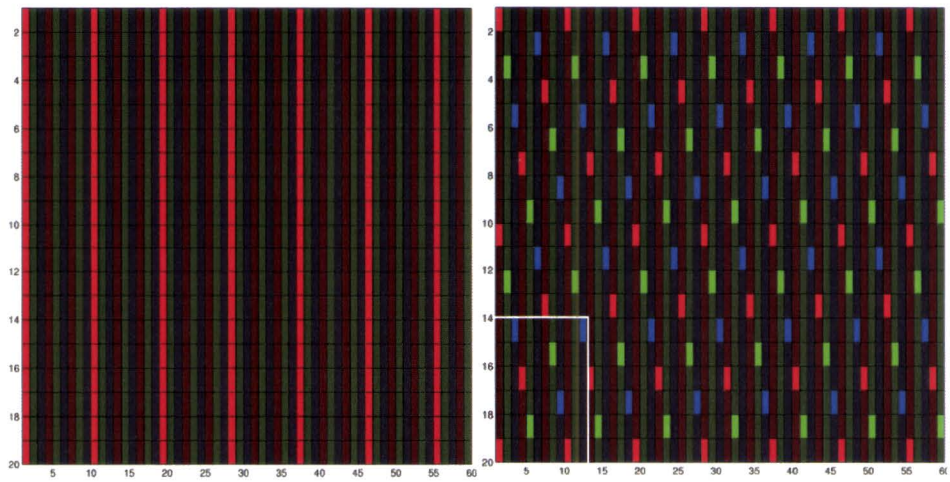

Figure 1.5: Sub-pixel layout of a 9 views 3D display. The left side shows all the sub-pixels that contribute to one view when the lenticular is vertically aligned. The right side shows the sub-pixels that contribute to one view when a slant angle of $\arctan(\frac{1}{6})$ is applied.

is distributed over both the horizontal and vertical direction. The right part of figure 1.5 shows the sub-pixel layout of a 9 views 3D display, having a slanted lenticular. The bright sub-pixels contribute to the formation of 1 view only. In this example, the bright sub-pixels are distributed in both the horizontal and vertical direction. The resolution loss is by a factor of 3 in both the vertical and horizontal direction.

Figure 1.6 shows the sub-pixel layout in the lower left corner of the right part of figure 1.5 in detail. The lenticular, indicated by the diagonal lines, is placed under a slant angle of $\arctan(\frac{1}{6})$. The numbers indicated in the sub-pixels correspond to the 9 individual views.

The sub-pixels are symmetrically positioned below a cylindrical lens. All the sub-pixels with number 5 are symmetrically positioned below the symmetry axis of a cylindrical lens. Therefore, these sub-pixels are imaged right in front of the display, generating view number 5. All the sub-pixels numbered by 4 are positioned slightly to the left of the symmetric axis of a cylindrical lens. All these sub-pixels are imaged slightly to the right, generating view number 4. All the sub-pixels numbered by 3 are positioned even more to the left with respect to the symmetric axis of a cylindrical lens. All these sub-pixels are imaged further to the right, generating view number 3. In this way, an angular viewing zone is created, containing 9 successive views (see also figure 1.1 for an angular viewing zone containing 5 views).

An LCD imaging 2D content with a lenticular placed in front of the display introduces yet another problem. The lens effect created by the lenticular makes text difficult to read and fine textures will not be displayed correctly. As a result, a 3D display is not suitable for normal monitor applications. However,

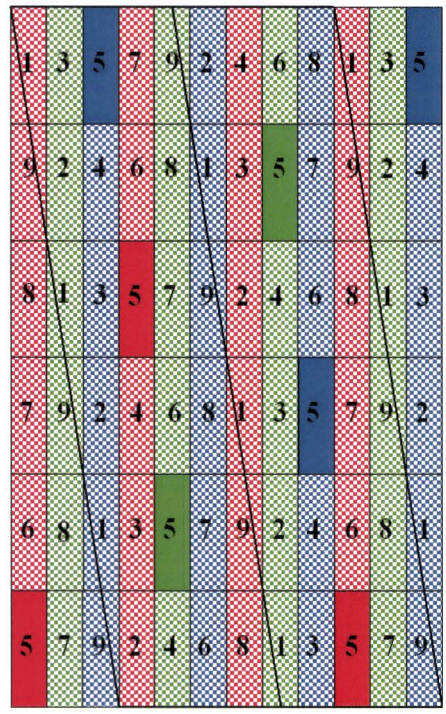

Figure 1.6: Sub-pixel layout of a 9 views 3D display with the lenticular under a slant angle of $\arctan(\frac{1}{6})$.

if the lens effect of a lenticular could somehow be switched on and off, a 3D display could be used for both 2D and 3D applications.

A pragmatic solution is the construction of a lenticular filled with a medium that can somehow be switched between two refractive states. The material that meets these requirements the most is liquid crystal (LC). In 2004, Philips Research succeeded in producing a switchable 2D/3D display based on liquid crystal lenses [3]. These liquid crystal lenses can be electronically switched between a refracting mode (3D mode) and a non-refracting mode (2D mode).

Liquid crystal can be considered as a liquid in which an ordered arrangement of molecules exists. Liquid crystals arise in organic substances having anisotropic molecules, that is, rod-like molecules or disk-like molecules. Rod-like molecules are uniaxially symmetric. The relative dielectric constants differ in value along the preferred axis, the director, ($\varepsilon_{||}$) and perpendicular to this axis ($\varepsilon_{\perp}$). The dielectric anisotropy is defined as

$$\triangle\varepsilon = \varepsilon_{||} - \varepsilon_{\perp}. \tag{1.1}$$

Because of the static dielectric anisotropy, it is possible to control the LC orientation with the help of an electric field.

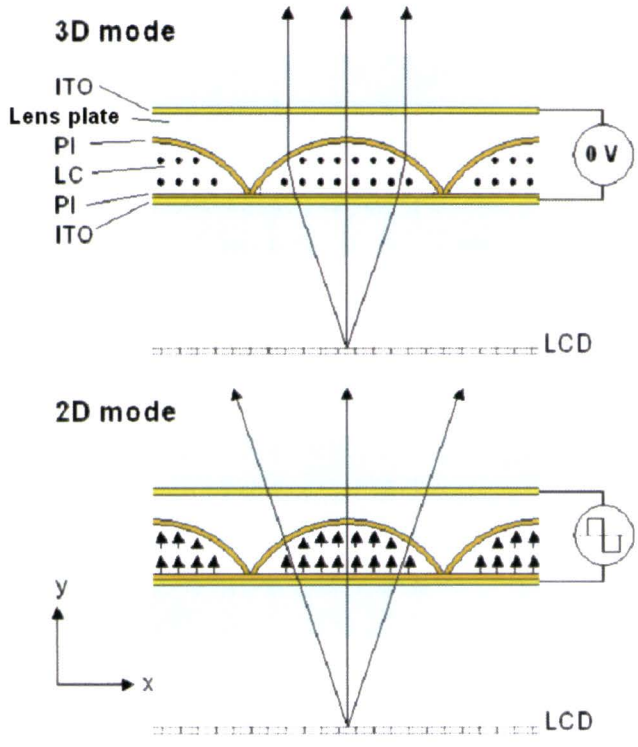

Figure 1.7: The two modes of a switchable lenticular. The 2D mode has no lens effect, since there is an index match between the lens and the lens plate. The 3D mode generates a positive lens effect.

Also in the optical regime, there is a dielectric anisotropy. The index of refraction n is related to the relative dielectric constant through

$$\varepsilon = n^2. \tag{1.2}$$

The index of refraction corresponding to $\varepsilon_\perp$ is the ordinary index of refraction n_o. The index of refraction corresponding to $\varepsilon_{||}$ is the extraordinary index of refraction n_e. The ordinary index of refraction applies for light with electric field polarization perpendicular to the director. The extraordinary index of refraction applies for light with electric field polarization parallel to the director. A medium having these properties is said to be uniaxially birefringent. The birefringence (or optical anisotropy) is defined as

$$\triangle n = n_e - n_o. \tag{1.3}$$

If $n_o < n_e$, the liquid crystal is said to be positive birefringent, whereas if $n_e < n_o$, it is said to be negative birefringent. [4][5][6]

Figure 1.7 shows a lenticular that contains liquid crystal. The lenticular consists of two glass plates that are equipped with a transparent conducting ITO (Indium Tin Oxide) layer. In between is a lens plate that contains an inverse

lens, molded out of a replica material. The remaining space is filled with liquid crystal.

On the lens plate and the lower glass plate a monolayer of poly-imide (PI) is applied. Rubbing of the PI surface is an effective way of achieving a preferred orientation of the PI molecules. The LC molecules orient themselves along the rubbing direction of the PI layer, occupying the lowest energy state.

The lower part of figure 1.7 shows the 2D mode of the switchable lenticular. A voltage is applied on the ITO layers creating an electric field in the y-direction. The LC molecules will align along the electric field lines, occupying the lowest possible energy state. As a result, the director is in the y-direction. The polarization direction of the light coming from the LCD is linearly polarized. If the polarization of the display is in the z-direction, the lens can be characterized having the ordinary index of refraction n_o. The light will not be refracted, since there is an index match between the lens and the lens plate. Consequently, there is no lens effect.

The upper part of figure 1.7 shows the 3D mode of the switchable lenticular. Here, the rubbing direction of the lens plate, the rubbing direction of the lower glass plate and the polarization of the display are in the z-direction. As a result, the lens, although being optically birefringent, can be approximated as an isotropic lens with index of refraction n_e. A positive lens effect is generated since the LC used in this application is positive birefringent.

With the possibility to switch between a 2D mode and a 3D mode, the user can choose according to its needs. However, there are some issues concerning the image quality in both the 2D mode and 3D mode. These issues will be discussed in the next section.

1.3 Performance limitations of 2D/3D switchable displays

The use of a lenticular introduces some imperfections in the performance of 2D/3D switchable displays. These imperfections can be characterized by two quality parameters: modulation depth and crosstalk. [7][8][9]

1.3.1 Modulation depth

The non-bright area of the sub-pixels of an LCD is called the black matrix. In the 3D mode of a switchable 2D/3D display, this black matrix is imaged at the viewing distance. The viewer experiences this effect as dark bands when viewing the display. Figure 1.8 shows the effect of dark bands. This disturbing artifact is enhanced by the fact that the dark bands are moving across the screen when the viewer moves from side to side in front of the display.

A measure for the variation in intensity output of a display is called the mod-

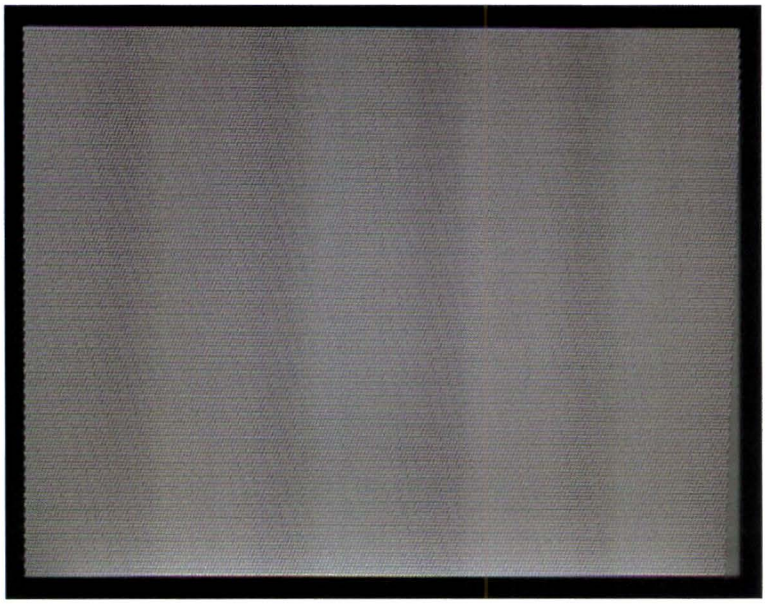

Figure 1.8: When viewing a 3D display, the viewer can see dark bands.

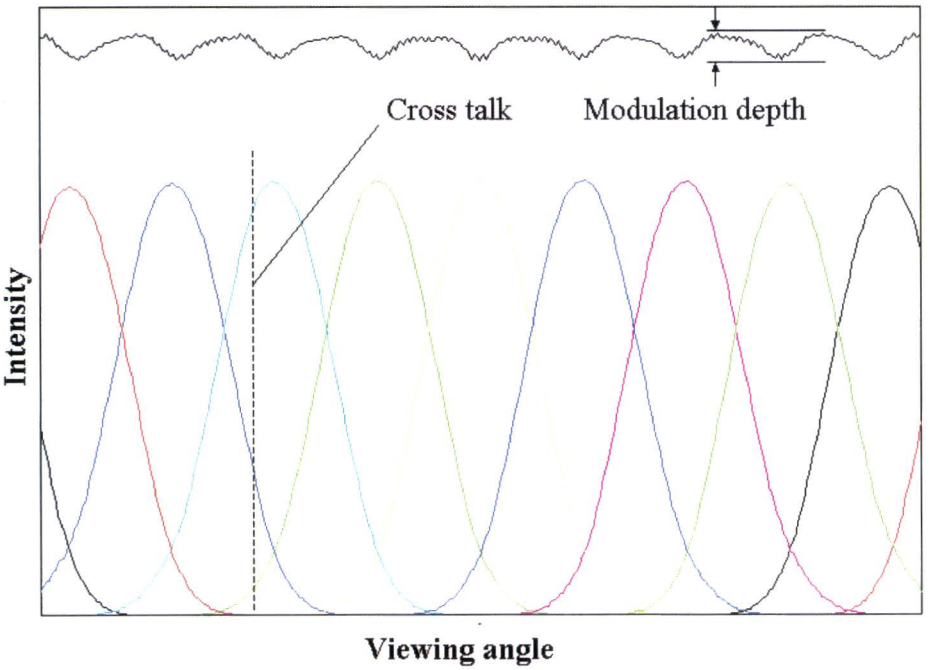

Figure 1.9: Angular distribution of 9 individual views. The total angular intensity distribution is depicted at the top of the figure.

ulation depth. The modulation depth M_d is defined as

$$M_d = \frac{\overline{SD(I_{tot})}}{\overline{I_{tot}}}, \tag{1.4}$$

where $\overline{SD(I_{tot})}$ is the average Standard Deviation in the total angular intensity distribution and $\overline{I_{tot}}$ the average total angular intensity distribution.
In the 2D mode of a switchable 2D/3D display, there appears to be a relatively large modulation depth at a certain viewing angle. For this specific viewing angle, the focal point of the switchable lenses is exactly on the pixel structure of the LCD. In the 2D mode, it are these residual lens effects that we would like to get rid of.

1.3.2 Crosstalk

Figure 1.9 shows the angular distribution of 9 individual views. Note that for one particular viewing angle, the viewer can see three different views. One of these views is more visible than the others since each view has a different intensity.
In addition, the total angular intensity distribution depicted at the top of the figure is angular dependent.

A measure for the overlap between the views is called the crosstalk. The crosstalk O is defined as

$$O = \frac{\int F \cdot G}{\sqrt{\int F^2}\sqrt{\int G^2}}, \tag{1.5}$$

where F and G are the angular intensity distributions of individual neighboring views. For symmetric intensity distributions, the crosstalk reaches its maximum precisely between two neighboring views.
If the crosstalk is too large, there are no stereo pairs since the angular distribution of the views is too narrow. Then, no three-dimensional image can be perceived by the viewer.

1.4 Thesis outline

In chapter 2, we introduce an analytical model for the ideal design of a lenticular for which there is no crosstalk and modulation depth.
Next, the 3D mode of a 9 views switchable 2D/3D display based on liquid crystal lenses [3] is investigated using a ray tracing program, developed by Philips Research. With this tracing program, the optimal design for a cylindrical (or spherical) lenticular is examined [7][8][9].
In order to decrease crosstalk and modulation depth in a 2.2 inch 5 views switchable 2D/3D display, we introduce the concept of a-spherically shaped lenses. With the tracing program, we investigate the optimal design of an a-spherical lenticular.

Figure 1.10: 9 views 20 inch switchable 2D/3D lenticular based display.

To investigate the 2D mode of a switchable display, it is necessary to introduce some theory describing the birefringent properties of liquid crystal [10].
Using this theory as a basis, we derive the refraction and reflection at liquid crystal interfaces in chapter 3.

In chapter 4, we analyze the 2D mode of a 9 views 20 inch switchable 2D/3D display by introducing a model that describes the angular dependency of the modulation depth in the 2D mode.
Figure 1.10 shows a 9 views 20 inch demonstrator, developed by Philips Research and presented at the International Display Workshop (IDW) in Japan in 2004 [1].
We introduce the idea of a birefringent lens plate as a possible solution to shift large modulation depths towards larger viewing angles.
We propose possible birefringent properties of the lens plate that are needed for this idea to work successfully.

Finally, in chapter 5, we investigate the 2D mode of a 9 views 20 inch switchable 2D/3D display using ray tracing.
We transform the theory described in chapter 3 into an algorithm and implement this in existing ray tracing software.

We analyze the tracing results and compare these to the analytic results of chapter 4. We also compare tracing results of the birefringent lens plate with the results of chapter 4.

In the last chapter, we formulate the main conclusions on the subject of a-spherical lenses and birefringent lens plates. In addition, we evaluate the theory introduced in chapter 3 that is used for the model in chapter 4 and the ray tracing in chapter 5 and examine the opposed conditions. Finally, we make some suggestions for future research.

In this thesis work, we have extended the state of the art with the concept of a-spherical lenticulars in chapter 2 and birefringent lens plates in chapter 4 and chapter 5. For the investigation of these subjects, we developed a ray tracing algorithm, based on the derived theory in chapter 3.

2

Analytical model and numerical ray tracing of 3D mode

In the previous chapter, two quality parameters of a 2D/3D switchable display have been introduced, namely modulation depth and crosstalk. Both the modulation depth and the crosstalk should be small in order to have a good image quality. The modulation depth and crosstalk depend on the optical design of the lenticular. This chapter concentrates on the optical design of a switchable lenticular in the 3D mode.

First, we determine the optimal design of an ideal cylindrical lenticular analytically. For this optimal design, there exists no modulation depth and crosstalk. Subsequently, the optimal design of a cylindrical lenticular is examined using a ray tracing program, developed by Philips Research. Obviously, there is a modulation depth and crosstalk for non-ideal spherical lenses. In order to reduce modulation depth and crosstalk, we examine the modulation depth and crosstalk of an a-spherical lenticular. We propose the design of an a-spherical lenticular to improve the 3D performance of a 2.2 inch 5 views switchable 2D/3D display.

2.1 Optical design of lenticular based display

Figure 2.1 shows the main parameters that need to be considered when constructing a lenticular based display. L is the viewing distance. The sub-pixel pitch is indicated by p and q is the distance between the viewer's eyes. The distance d/n is the optical distance between the sub-pixels and the lenticular, where it is assumed that $p \ll d$. Here, n is the index of refraction of the medium involved. B is the pitch of the cylindrical lenses.
For a correct angular distribution of the views of a lenticular based display, the pitch B of the lenses should be chosen carefully.
The lenticular should be designed in such a way, that all the corresponding views are depicted in the same area at the viewing distance. For example, the

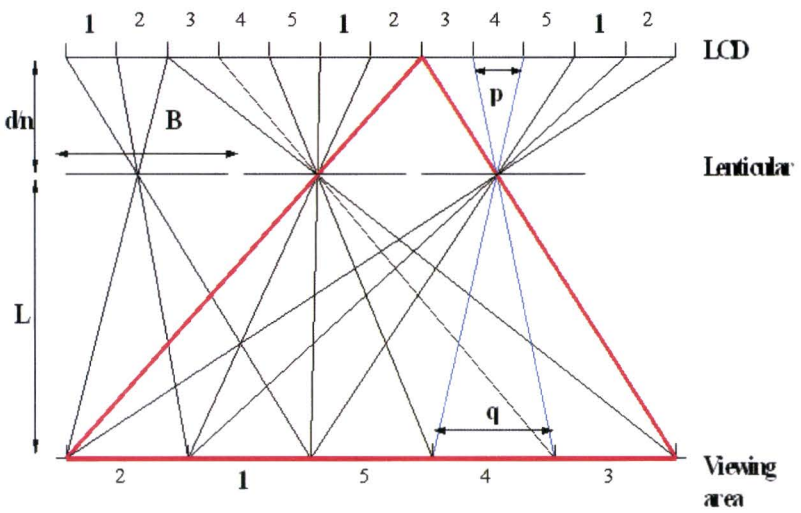

Figure 2.1: A 5 view lenticular based display with viewpoint correction.

images of the sub-pixels indicated by 1 in figure 2.1 must overlap each other completely in the viewing area. This is called a viewpoint correction.

A viewpoint correction can be realized by adjusting the lens pitch B. Given the geometry in figure 2.1, it is possible to derive an expression for the correct lens pitch B.
Considering equally shaped triangles, depicted in blue in figure 2.1, the relation between p, q, L and d is given by

$$\frac{L}{q} = \frac{\frac{d}{n}}{p}. \tag{2.1}$$

Next, consider the red triangle indicated in figure 2.1. For a system containing N views, B is given by

$$\frac{B}{\frac{d}{n}} = \frac{Nq}{L + \frac{d}{n}}. \tag{2.2}$$

Using equation 2.1, B can be written as

$$B = N\frac{pq}{p+q}. \tag{2.3}$$

One would expect the lenses to have a focal distance f_0 for which the image of a point source at the pixel structure is exactly in focus with the viewing distance. However, this is not desirable, since the black matrix would also be imaged exactly at the viewing distance, generating a high modulation depth. The intensity distribution would be non-uniform, creating dark bands in the display.
Rather than designing an ideal focal distance f_0, the focal distance is designed in such a way that the images of point sources at the pixel structure are blurred

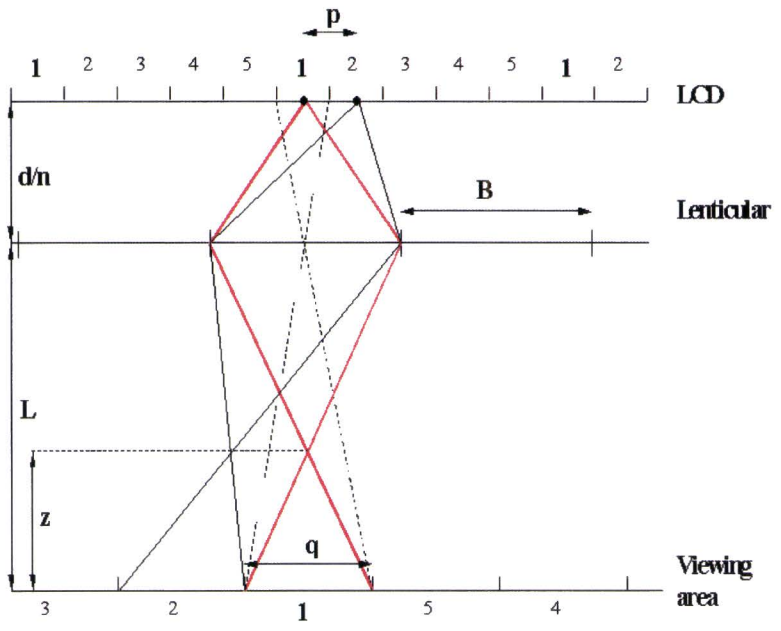

Figure 2.2: Relevant geometries concerning the optimal focal distance f.

at the viewing distance. If the focal distance of the lenses is chosen properly, the intensity distribution of the imaged point sources at the viewing area is uniform. In this case, we get rid of the dark bands.

Figure 2.2 shows a situation for which this is exactly the case. Consider two point sources with a mutual distance p, shown in figure 2.2. The images of these point sources are positioned exactly side by side, creating a uniform intensity distribution.
Using the geometries indicated in figure 2.2, it is possible to derive an expression for the focal distance f. To begin with, it is easily derived that

$$\frac{q}{z} = \frac{B}{L-z}. \tag{2.4}$$

Using the thin lens equation, the focal distance f is related to d, L and z by

$$\frac{1}{f} = \frac{1}{\frac{d}{n}} + \frac{1}{L-z}. \tag{2.5}$$

Substituting equation 2.3 and 2.4 in equation 2.5, eliminating z and rearranging terms results in an expression for the focal distance

$$f = f_0 \frac{1}{1+\frac{1}{N}}, \tag{2.6}$$

with

$$f_0 = \frac{\frac{d}{n}q}{p+q}. \tag{2.7}$$

Obviously, if $z = 0$, the focal distance f_0 is the ideal focal distance for which the point sources are exactly in focus with the viewing distance. For $z \neq 0$, the images of the point sources at the viewing distance are blurred.

The focal distance stated in equation 2.6 is not the only focal distance for which a uniform intensity distribution exists. Other focal distances can be derived in the same way equation 2.6 is derived.
Consider two point sources with a mutual distance of mp, with m an integer. It can be derived that the focal distance f_m is now given by

$$f = f_0 \frac{1}{1 + \frac{m}{N}}, \qquad m \in \mathbb{Z}|_{\{0\}}. \tag{2.8}$$

Values for $m < 0$ and $m > 0$ indicate focal distances that correspond to over and under focus respectively.

The derivation described above, is valid for all pairs of point sources having a mutual distance mp. If we would integrate over all these pair contributions, the total intensity output would still be uniform.

The actual design parameter is the radius of curvature R of a lens, which determines the focal distance f. The focal distance of a thin lens with a spherical surface and a flat surface is related to the radius of curvature according to [4]

$$\frac{1}{f} = (n_{lens} - 1)\frac{1}{R}, \tag{2.9}$$

where it is assumed that the lens is used in air. Using 2.9, equation 2.8 can also be written as

$$R = R_0 \frac{1}{1 + \frac{m}{N}}, \qquad m \in \mathbb{Z}|_{\{0\}}, \tag{2.10}$$

with

$$R_0 = \frac{\frac{d}{n} q (n_{lens} - 1)}{p + q}. \tag{2.11}$$

If $m = 0$, the radius of curvature R would be the ideal radius of curvature R_0, corresponding to the focal distance f_0, for which the dark bands are visible.

If the pitch B of the ideal lenses is given by equation 2.3, there is no crosstalk between the views. If the radius of curvature R is given by equation 2.10, there is no modulation depth in the total angular intensity distribution of a 3D display. This is achieved by de-focussing of the lenticular. Under these conditions, the 3D performance of a 3D display is perfect.

2.2 Modulation depth and crosstalk of spherical lenticular

In reality, a 2D/3D switchable display in the 3D mode does have a modulation depth and crosstalk. If we want to investigate the modulation depth and

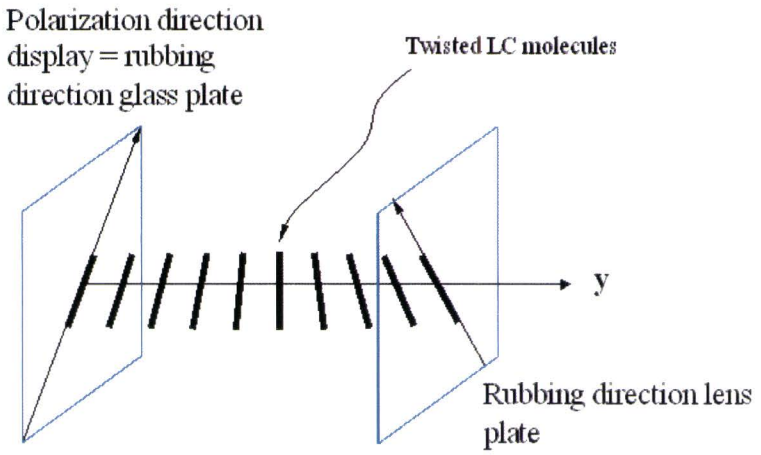

Figure 2.3: Cell containing twisted LC material (3D mode). If the cell is thick enough, the polarization direction of the light travelling in the y-direction is rotated clockwise. Since the polarization direction is aligned with the director at any point in the LC cell, the current index of refraction is n_e.

crosstalk in detail, it is helpful to use ray tracing. Ray tracing is a technique to determine the actual path of individual rays of light through an optical system. Each ray can be traced, independently, using only the laws of refraction and reflection together with geometry.
With the help of a ray tracing program, the necessary calculations yielding the changes in position and direction of a ray is done more easily and quickly and without approximations concerning lens aberrations. The tracing program that is used in this chapter requires a well defined optical geometry. Additionally, the program has to be modified to some extent in line with the required output.

The tracing program for the lenticular in the 3D mode not necessarily requires the implementation of birefringent properties. In order to understand this, consider the following argumentation.
In general, the switchable lenticular contains twisted LC material. This can be explained as follows. Consider figure 1.7. The rubbing direction of the PI layer of the lens plate is parallel to the long axis of the cylindrical lenses. The rubbing direction of the PI layer of the lower glass plate should match the polarization direction of the light coming from the LCD, which in general is not parallel to the rubbing direction of the lens plate. The LC molecules will orient themselves along the rubbing directions, creating a rotation in the direction of the directors. This rotation is also known as twist. Figure 2.3 shows a cell that contains twisted LC molecules.
The polarization direction of the light coming from the display will be rotated along with the twist of the LC molecules when travelling through the LC material. This effect is called strong guiding [10]. The polarization direction of the light coming from the display is parallel to the director at any position in the LC cell. As a result, the light travelling in the y-direction will experience

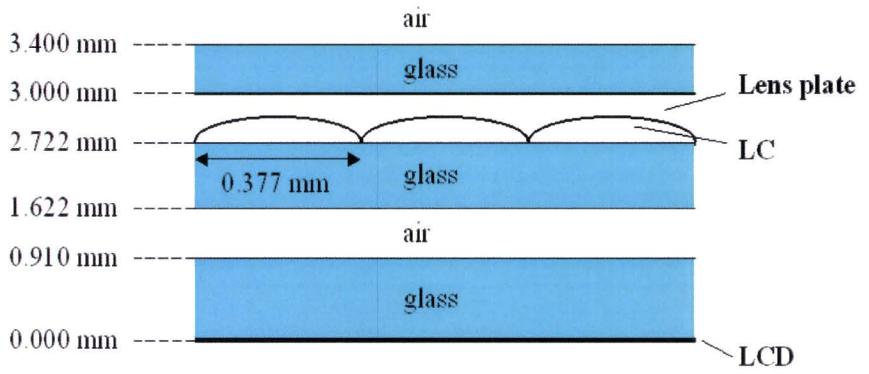

Figure 2.4: Geometry of a 9 views 20 inch switchable lenticular based display.

an extraordinary index of refraction n_e.
It is concluded that the switchable lenticular in the 3D mode can be approximated by an isotropic lens with index of refraction n_e. Here, it is assumed that the light is travelling in the y-direction (see figure 2.3). Note that the optical properties become totally different if the light is propagating under oblique angles.

We use the geometry of a 9 views 20 inch switchable 2D/3D lenticular based display as an example. The geometry which is placed in front of the LCD is depicted in figure 2.4.
The horizontal and vertical sub-pixel pitches p are 0.085 millimeter and 0.255 millimeter, respectively. The non-bright fraction in horizontal direction is 43% and 31% in vertical direction. The slant angle of the lenticular is $\arctan(\frac{1}{6})$. The type of liquid crystal used in this system is TL213 with an ordinary index of refraction of 1.527 and an extraordinary index of refraction 1.766. The index of refraction of glass is 1.500 and the index of refraction of the lens plate material (polymer) is 1.550.
We determine the modulation depth and the crosstalk as a function of the radius of curvature R of the spherical lenticular using the ray tracing program. In figure 2.5a, the crosstalk for two neighboring views is depicted. The crosstalk of two next neighboring views and two next next neighboring views are depicted in figure 2.5b and 2.5c, respectively. As one would expect, the crosstalk of two next neighboring views is lower than the crosstalk of two neighboring views. Figure 2.5d shows the resulting modulation depth.

If we examine figure 2.5, we find out that the interval for which the crosstalk is low appears to have a large modulation depth. In addition, the interval for which the modulation depth is relatively small appears to have a high crosstalk. Somehow, a radius of curvature R has to be chosen for which an acceptable balance between crosstalk and modulation depth exists. For example, $R = 0.422$ millimeter results in a cross talk of 0.386 and a modulation depth of 0.013 and $R = 0.519$ millimeter results in a cross talk of 0.373 and a modulation depth of

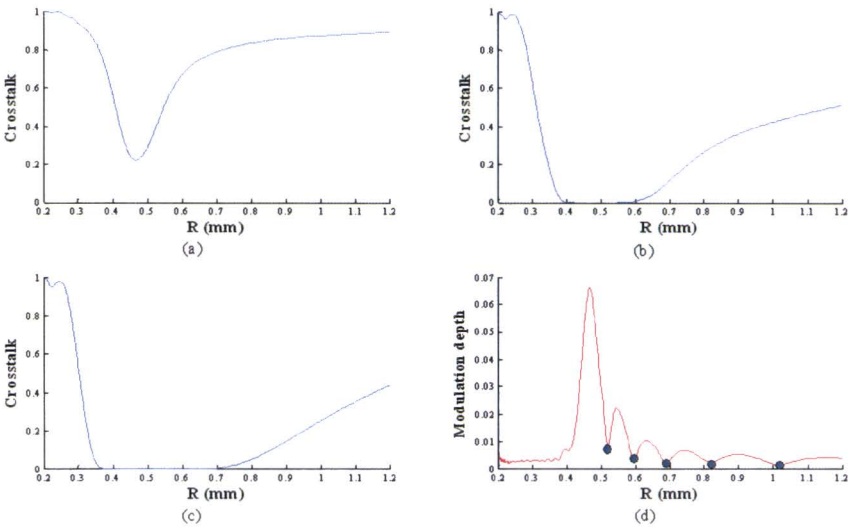

Figure 2.5: a) Ray tracing results for crosstalk of two first neighboring views. b) crosstalk of two next neighboring views. c) crosstalk of two next next neighboring views. d) modulation depth.

0.008. These are typical values for R, the crosstalk and the modulation depth when considering the design for a 9 views 20 inch switchable 2D/3D display.

Consider figure 2.5d. The high peak corresponds to a radius of curvature, for which the image of the black matrix is in focus with the viewing area, generating a large modulation depth. The radii of curvature with a relatively low modulation depth are indicated by the blue dots. These radii of curvature correspond to $m = -1$, $m = -2$ etc. in equation 2.10. The radii of curvature for $m = -1$ and $m = -2$ according to equation 2.10 are $R = 0.482$ millimeter and $R = 0.551$ millimeter, respectively.
If we compare the tracing results in figure 2.5d with these analytical results, we find out that they do not match.
Most likely, the miss match between ray tracing results and analytical results is due to lens aberrations. The analytical description of the lenticular assumes an ideal thin lens, having no lens aberrations, whereas the lenticular defined in the ray tracing program does include lens aberrations.

It can be concluded that by slightly de-focussing of the lenticular, slightly more crosstalk is permitted, resulting in a less intense modulation depth.

2.3 Modulation depth and crosstalk of a-spherical lenticular

At the beginning of the thesis project, in December 2004, a 5 views switchable display was a possible application for mobile phone displays [3]. The occurrence

of dark bands was one of the big issues. In order to reduce the dark bands, we suggested the use of an a-spherically shaped lenticular in order to improve the 3D performance. We investigated the concept with the help of the tracing program of section 2.2 in which we defined a-spherically shaped lenticulars.

In this section, we investigate the lenticular design for a 2.2 inch 5 views 2D/3D switchable display. The horizontal and vertical sub-pixel pitches p are 0.046 millimeter and 0.138 millimeter, respectively. The non-bright fraction in horizontal direction is 32% and 59% in vertical direction. The slant angle of the lenticular is $\arctan(\frac{1}{3})$. The type of liquid crystal used in this system is TL213 with $n_o = 1.527$ and $n_e = 1.766$. The index of refraction of glass is 1.500 and the index of refraction of the lens plate material is 1.527. the optical thickness between the sub-pixels and the lenticular is 1.187 millimeter and the pitch B of the lenses is 0.218 millimeter.
We performed the same ray tracing calculations as in section 2.2, concerning the modulation depth and crosstalk. This time, we present the crosstalk as a function of the modulation depth, depicted by the blue dots in figure 2.6. Each blue dot represents a radius of curvature R. The values for R are between 0.2 and 0.9 millimeter.

We prefer the blue dots to be as close to the origin as possible since in this region, they represent a low crosstalk and small modulation depth. The blue dot representing a radius of curvature of 0.25 millimeter is pointed out in figure 2.6. This dot is relatively close to the origin and has a crosstalk of 0.147 and a modulation depth of 0.028.
We hope to improve the modulation depth and crosstalk for $R = 0.25$ millimeter by introducing a-spherically shaped lenticulars.

In order to describe an a-spherical lens, we first expand a function describing spherical lenses in a Taylor series. A spherical lens with radius of curvature R and lens pitch B is described by

$$F(x) = \sqrt{R^2 - x^2} - \sqrt{R^2 - (\frac{B}{2})^2}, \tag{2.12}$$

with $-\frac{B}{2} \leq x \leq \frac{B}{2}$ and $\frac{B}{2} \leq R$. This equation can also be written as

$$F(x) = R\sqrt{1 - \frac{x^2}{R^2}} - \sqrt{R^2 - (\frac{B}{2})^2}. \tag{2.13}$$

If $\frac{|x|}{R} < 1$, equation 2.13 can be expanded in a series. Then, the lens shape is given by

$$F(x) = R - \sqrt{R^2 - (\frac{B}{2})^2} + R\sum_{i=1}^{\infty}(-1)^i \frac{\alpha(\alpha-1)...(\alpha-i+1)}{i!}(\frac{x}{R})^{2i}|_{\alpha=\frac{1}{2}}. \tag{2.14}$$

The first four terms of this series are given by

$$F(x) = R - \sqrt{R^2 - (\frac{B}{2})^2} - \frac{1}{2}\frac{x^2}{R} - \frac{1}{8}\frac{x^4}{R^3} - \frac{1}{16}\frac{x^6}{R^5}. \tag{2.15}$$

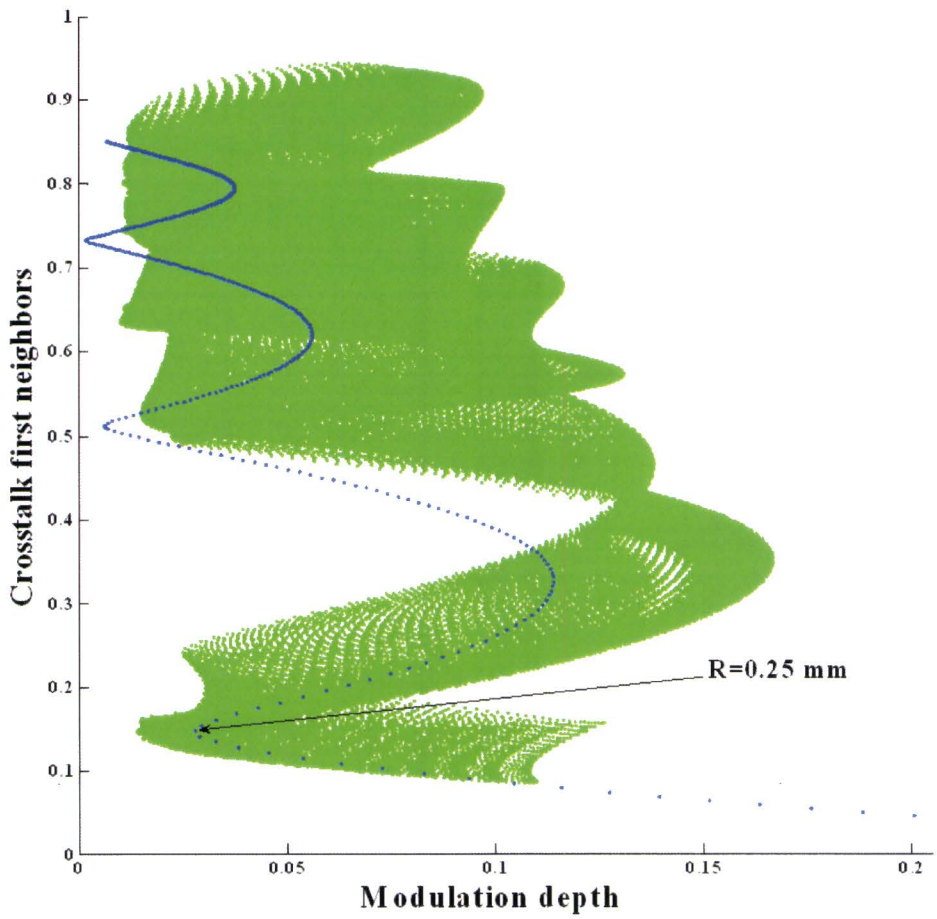

Figure 2.6: Ray tracing results of crosstalk and modulation depth of a 2.2 inch 5 views switchable display. The blue dots represent results for spherical lenticulars, whereas the green dots represent results for a-spherical lenticulars.

Note that the coefficients of the polynomial function depend on the radius of curvature.

Using a radius of curvature of 0.25 millimeter, equation 2.15 yields

$$F(x) = a - bx^2 - cx^4 - dx^6, \tag{2.16}$$

with $a = 0.025$, $b = 2.000$, $c = 8.000$ and $d = 64.000$. By varying the coefficients a, b, c and d around their initial values, we hope to create a lenticular having lower modulation depth and crosstalk. Each unique combination of coefficients will produce a new dot in figure 2.6. These dots are depicted in green.
Keeping c and d constant and varying b around the value 2, we determine a value for b for which the corresponding green dot is closer to the origin of figure 2.6. Then, by varying c around 8 and keeping b and d constant, we try to find a dot even closer to the origin. This can also be done for d, though variation of this parameter does not provide us with significantly better results. The

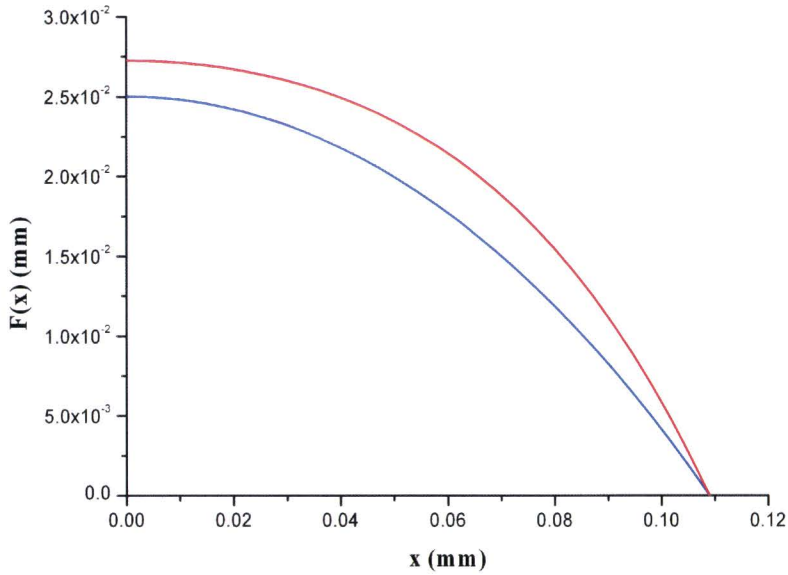

Figure 2.7: Cross-section ($0 \leq x \leq \frac{B}{2}$) of the spherical lenticular (blue) and the a-spherical lenticular (red).

green dot that we found to be as close to the origin as possible represents an a-spherical shape given by

$$F(x) = 0.027 - 1.320x^2 - 82.000x^4 - 0.000x^6. \tag{2.17}$$

An a-spherical lenticular given by equation 2.17 has a crosstalk of 0.146 and a modulation depth of 0.014. If this result is compared with the spherical lens with radius of curvature $R = 0.25$ millimeter, it appears that the modulation depth can be reduced by a factor of two, keeping the crosstalk nearly constant.

Figure 2.7 shows the cross-section of the lenticulars involved. The spherical lenticular with $R = 0.25$ millimeter is depicted in blue and the a-spherical lenticular with the shape given by equation 2.17 is depicted in red.

The shape of the a-spherical lens in figure 2.7 has steeper slopes at the edges than the spherical lens with $R = 0.25$ millimeter. As a consequence, optical aberrations of the a-spherical lens are increased with respect to the spherically shaped lenticular. With the presence of optical aberrations in a lenticular, it is possible to blur the images of a 3D display, reducing the modulation depth.
This can be explained by giving an example. Consider figure 2.8. The figure shows a lens with an incident beam of parallel rays. Depending on the aperture h of the lens, the rays are focussed to different points behind the lens. As a consequence, the image of the incident beam at a distance l from the lens is a blurred spot rather than an infinitely small spot. This effect is called spherical aberration.
Note that blurring can also be achieved by de-focussing the lenses, as discussed

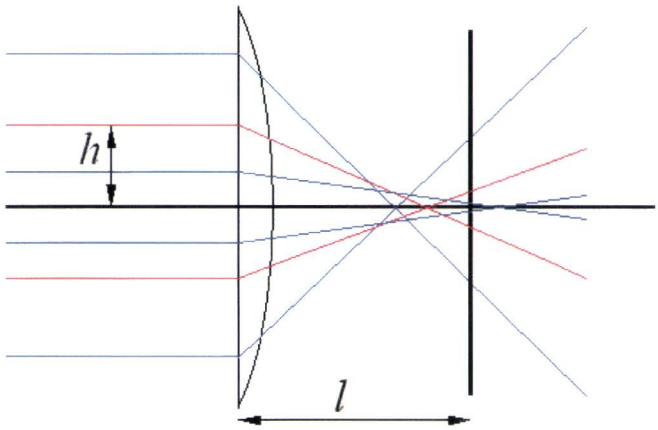

Figure 2.8: Spherical aberration of a lens, producing different focal lengths.

in section 2.1 and 2.2.

Based on the results described in this section, the idea of a-spherically shaped lenticulars proved to be one of the possible solutions for reducing the effect of dark bands. Therefore, we tried to claim the idea writing an invention disclosure. However, the request was rejected, since it would be extremely difficult to formulate a generic claim without covering arrangements which may have been disclosed before. As a result, the subject of a-spherically shaped lenticulars is best kept as knowhow.

We conclude this chapter with the following statements. The modulation depth of a 2D/3D switchable lenticular based display can be reduced by de-focussing of the spherically shaped lenticular. In order to reduce the modulation depth even more, the concept of a-spherically shaped lenticulars proved to be a possible solution. It appears that the use of a-spherically shaped lenticulars is equivalent to an increase in lens aberrations. Therefore, it can be concluded that additional lens aberrations can improve the 3D performance of a switchable 2D/3D lenticular based display.

3

Refraction and reflection of light at birefringent media

Unlike the 3D mode, described in chapter 2, the 2D mode of a switchable lenticular cannot be regarded as a lens which is optically isotropic. The birefringent optical properties of the 2D mode depend on the direction of propagation and the polarization direction of the light relative to the orientation of the LC molecules inside the switchable lenticular. Before we can actually investigate the 2D mode of a 2D/3D switchable lenticular based display, we need to introduce some theory concerning birefringent media.
First, the optical properties of birefringent media are deduced from Maxwell's equations [10]. Then, we work out these properties for refraction and reflection of light at plane liquid crystal interfaces. In addition, we explain how this can be used for the investigation of the 2D mode of a 2D/3D switchable lenticular based display.

3.1 Light propagation in birefringent media

The most fundamental equations in electrodynamics are Maxwell's equations. These are given by [11]:

$$\nabla \times \mathbf{E} + \frac{\partial \mathbf{B}}{\partial t} = 0, \tag{3.1}$$

$$\nabla \times \mathbf{H} - \frac{\partial \mathbf{D}}{\partial t} = \mathbf{J}, \tag{3.2}$$

$$\nabla \cdot \mathbf{D} = \rho, \tag{3.3}$$

and

$$\nabla \cdot \mathbf{B} = 0. \tag{3.4}$$

In these equations, $\mathbf{E}$ and $\mathbf{H}$ are the electric field vector (V/m) and the magnetic field vector (A/m), respectively. The quantities $\mathbf{D}$ and $\mathbf{B}$ are the electric displacement (C/m^2) and the magnetic induction (Wb/m^2), respectively. The quantities ρ and $\mathbf{J}$ are the electric charge density (C/m^3) and the current density (A/m^2), respectively, and may be considered as the sources of the fields $\mathbf{E}$

and **H**.

In optics of birefringent media, the propagation of electromagnetic waves are described in regions of space where both the electric charge density and current density are zero. Therefore, it is allowed to set ρ=0 and **J**=0.

Maxwell's equations are completed with the material equations:

$$\mathbf{D} = \underline{\underline{\varepsilon}}\mathbf{E} \tag{3.5}$$

$$\mathbf{B} = \underline{\underline{\mu}}\mathbf{H} \tag{3.6}$$

The parameters $\underline{\underline{\varepsilon}}$ and $\underline{\underline{\mu}}$ are the electric tensor and the permeability tensor, respectively. If the medium is optically isotropic, both $\underline{\underline{\varepsilon}}$ and $\underline{\underline{\mu}}$ reduce to scalars.

The wave propagation is determined by the dielectric tensor ε_{ij} given by

$$D_i = \varepsilon_{ij} E_j. \tag{3.7}$$

In nonmagnetic and transparent materials, this tensor is real and symmetric, which implies $\varepsilon_{ij} = \bar{\varepsilon}_{ji}$.
It is always possible to find three orthogonal axes in such a way that the off-diagonal elements are zero. Therefore, the dielectric tensor is given by

$$\varepsilon = \begin{pmatrix} \varepsilon_x & 0 & 0 \\ 0 & \varepsilon_y & 0 \\ 0 & 0 & \varepsilon_z \end{pmatrix} \tag{3.8}$$

where ε_x, ε_y, and ε_z are the relative principal dielectric constants. The x, y and z axes are the principal dielectric axes of the crystal structure of the birefringent medium. These axes form the principal coordinate system. The principal relative dielectric constants are related to the principal indices of refraction n_x, n_y and n_z by

$$\varepsilon_i = n_i^2, \qquad i = x, y, z. \tag{3.9}$$

To study the propagation of light along a general direction, a monochromatic plane wave is assumed with an electric field vector given by

$$\mathbf{E} \;\; exp(i(\omega t - \mathbf{k} \cdot \mathbf{r})), \tag{3.10}$$

and a magnetic field vector given by

$$\mathbf{H} \;\; exp(i(\omega t - \mathbf{k} \cdot \mathbf{r})), \tag{3.11}$$

with ω the frequency of the plane wave. The wave vector **k** can be written as

$$\mathbf{k} = \frac{\omega}{c} n\mathbf{s}, \tag{3.12}$$

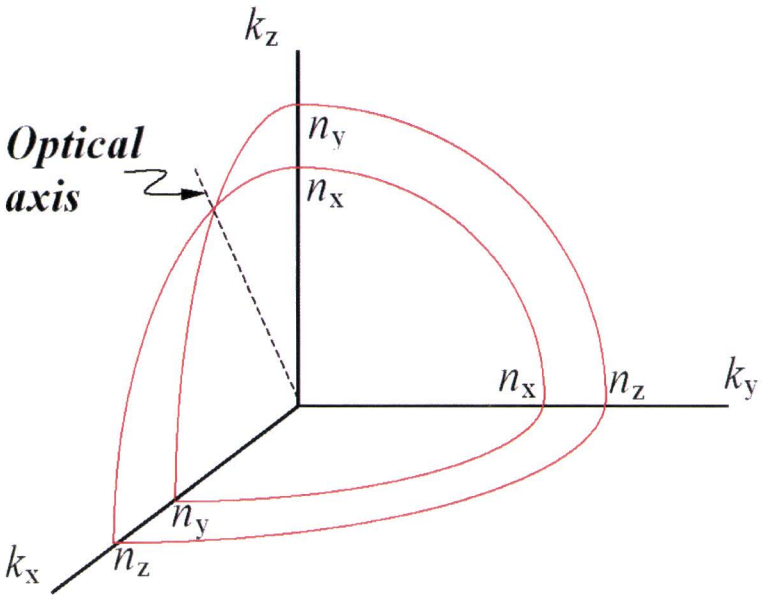

Figure 3.1: Octant of normal surface in **k** space with k_x, k_y and k_z in units of ω/c.

where **s** is a unit vector in the direction of the propagation, and c the speed of light. Substituting **E** and **H** in the Maxwell equations yields

$$\mathbf{k} \times \mathbf{E} = \omega\mu\mathbf{H} \tag{3.13}$$

and

$$\mathbf{k} \times \mathbf{H} = -\omega\mathbf{D}. \tag{3.14}$$

Eliminating **H** from equations 3.13 and 3.14 yields

$$\mathbf{k} \times (\mathbf{k} \times \mathbf{E}) + \omega^2\varepsilon\mu\mathbf{E} = 0. \tag{3.15}$$

This equation will be used to solve for the eigenvectors **E** and the corresponding eigenvalues n.

Using equation 3.8, equation 3.15 can be written as

$$\begin{pmatrix} \omega^2\mu\varepsilon_x - k_y^2 - k_z^2 & k_xk_y & k_xk_z \\ k_yk_x & \omega^2\mu\varepsilon_y - k_x^2 - k_z^2 & k_yk_z \\ k_zk_x & k_zk_y & \omega^2\mu\varepsilon_z - k_x^2 - k_y^2 \end{pmatrix} \begin{pmatrix} E_x \\ E_y \\ E_z \end{pmatrix} = 0. \tag{3.16}$$

This equation has only nontrivial solutions for the eigenvector **E** if the determinant of the matrix equals zero. This demand leads to a relation between ω and **k**.

For a given frequency ω, the relation between ω and $\mathbf{k}$ represents a three dimensional surface in $\mathbf{k}$ space. This surface is known as the normal surface and it consists of two shells. In general, these two shells have four points in common. The two lines that go through the origin and these points are known as the optical axes or the c axes. Figure 3.1 shows one octant of a general normal surface.

For each direction of propagation, there are two k values that are the intersections of the direction of propagation $\mathbf{s}$ and the normal surface. These two k values correspond to two different phase velocities (ω/k) of the waves propagating along the chosen direction. For propagation along the optical axis, there is only one value of k and therefore only one phase velocity.
Generally speaking, the two different phase velocities correspond to two normal modes of polarization. The directions of the electric field vector associated with these normal modes can be obtained from equations 3.16 and 3.12. This yields

$$\begin{pmatrix} E_x \\ E_y \\ E_z \end{pmatrix} = \begin{pmatrix} \frac{s_x}{n^2-n_x^2} \\ \frac{s_y}{n^2-n_y^2} \\ \frac{s_z}{n^2-n_z^2} \end{pmatrix}, \tag{3.17}$$

given that the denominators do not vanish. It is important to realize that in a non-absorbing medium, the normal modes are linearly polarized since all the components in equation 3.17 are real.
In addition, the determinant of the matrix in equation 3.16 must vanish and this yields

$$\frac{s_x^2}{n^2-n_x^2} + \frac{s_y^2}{n^2-n_y^2} + \frac{s_z^2}{n^2-n_z^2} = \frac{1}{n^2}. \tag{3.18}$$

Equation 3.18 is known as Fresnel's equation of wave normals and can be solved for the eigenvalues of index of refraction. For each direction of propagation, two solutions can be obtained. Each solution determines an electric field vector.

In order to derive the solutions for the eigenvalues of index of refraction for birefringent media, it is necessary to determine the corresponding normal surface.

If $\mathbf{k}$ is in units of ω/c, the normal surface is determined by the principal indices of refraction. When these are all different, there are two optical axes. In this case, the medium is biaxial (see figure 3.1).
A medium is uniaxially birefringent if two of the principal indices of refraction are equal. The index of refraction that corresponds to the two equal elements is called the ordinary index of refraction, for which $n_x = n_y = n_o$. The remaining index of refraction is called the extraordinary index of refraction, for which $n_z = n_e$.
If all three principal indices are equal, the two shells degenerate to a single sphere and the medium is optically isotropic.

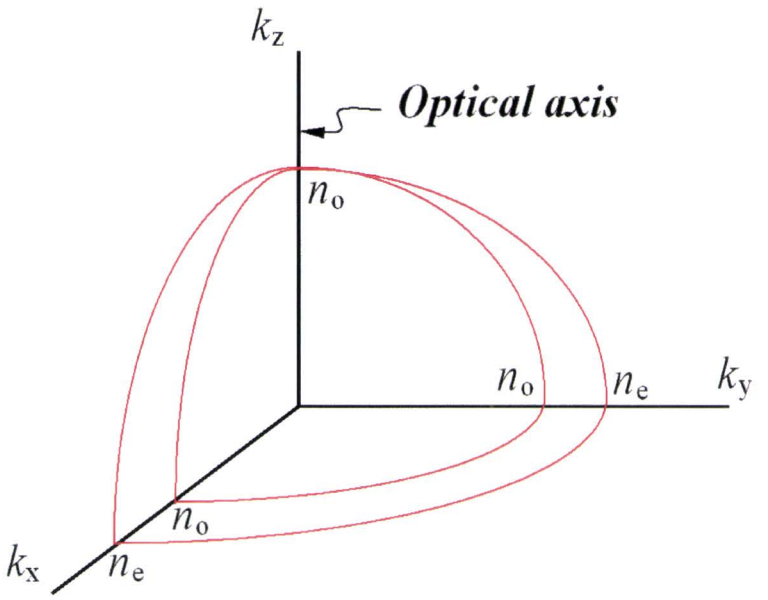

Figure 3.2: Octant of normal surface for a uniaxially birefringent medium in **k** space with k_x, k_y and k_z in units of ω/c and with $n_x = n_y = n_o$ and $n_z = n_e$.

For uniaxially birefringent media, the normal surface is given by

$$(\frac{k_x^2 + k_y^2}{n_e^2} + \frac{k_z^2}{n_o^2} - \frac{\omega^2}{c^2})(\frac{\mathbf{k} \cdot \mathbf{k}}{n_o^2} - \frac{\omega^2}{c^2}) = 0. \tag{3.19}$$

The normal surface is depicted in figure 3.2. The figure shows that the normal surface consists of a sphere and an ellipsoid of revolution. Both surfaces touch at two points on the z-axis. The z-axis is therefore the only optical axis. The sphere gives the relation between ω and **k** of the ordinary (O) wave. The ellipsoid of revolution gives the relation between ω and **k** for the extraordinary (E) wave.

By transforming the components of the unit vector **s** in sphere coordinates and by substituting equation 3.12 in equation 3.19, the eigen refractive indices associated with the E and O waves can be deduced.
The eigen refractive index for the E wave is given by

$$\frac{1}{n^2} = \frac{cos^2\theta}{n_o^2} + \frac{sin^2\theta}{n_e^2}, \tag{3.20}$$

where θ is the angle between the direction of propagation and the optic axis. The eigen refractive index for the O wave is given by

$$n = n_o. \tag{3.21}$$

The direction of the electric field vector $\mathbf{E}_e$ of the E wave can be obtained from equation 3.17 and is given by

$$\mathbf{E}_e = \begin{pmatrix} \frac{s_x}{n^2-n_o^2} \\ \frac{s_y}{n^2-n_o^2} \\ \frac{s_z}{n^2-n_e^2} \end{pmatrix}, \tag{3.22}$$

where n is as given by equation 3.20. $\mathbf{E}_e$ is not exactly perpendicular to the direction of propagation (s_x, s_y, s_z).
The direction of the electric field vector $\mathbf{E}_o$ for the O wave cannot be obtained from equation 3.17, because the denominators vanish when n is given by equation 3.21. Consequently, it must be obtained from equation 3.16. By using $\mathbf{k}_o = (\omega/c)n_o\mathbf{s}$, equation 3.16 can be written as

$$\begin{pmatrix} s_x^2 & s_x s_y & s_x s_z \\ s_y s_x & s_y^2 & s_y s_z \\ s_z s_x & s_z s_y & \frac{n_e^2}{n_o^2} - s_x^2 - s_y^2 \end{pmatrix} \mathbf{E}_o = 0. \tag{3.23}$$

The direction of polarization for the O wave leading from this equation is given by

$$\mathbf{E}_o = \begin{pmatrix} s_y \\ -s_x \\ 0 \end{pmatrix}. \tag{3.24}$$

The electric field vector for the O wave is perpendicular to the plane formed by the wave vector $\mathbf{k}_o$ and the optical axis $\mathbf{c}$, since $\mathbf{E}_o \cdot \mathbf{s}$ and $\mathbf{E}_o \cdot \mathbf{c}$ both equal zero.

Note that the polarization directions $\mathbf{E}_o$ and $\mathbf{E}_e$ are orthogonal, since the inner product of $\mathbf{E}_o$ with $\mathbf{E}_e$ is zero.

3.2 Refraction and reflection at liquid crystal interfaces

In order to examine the birefringent properties of the 2D mode, it is sufficient to investigate the refraction and reflection of light at plane liquid crystal interfaces. This is because refraction or reflection of light at a curved surface is determined by the tangent plane at the point of intersection.

Consider the plane boundary depicted in figure 3.3. The upper part of the figure is a medium which is optically isotropic with index of refraction n_i. The lower part is a positive birefringent medium. We consider a linearly polarized incident plane wave. The incident wave vector $\mathbf{k}_i$ will be refracted at the boundary. The boundary condition for reflection and refraction at a plane boundary requires that the magnitude of the tangential component of the wave vector along the boundary is conserved. In addition, all wave vectors lie in the plane of incidence.

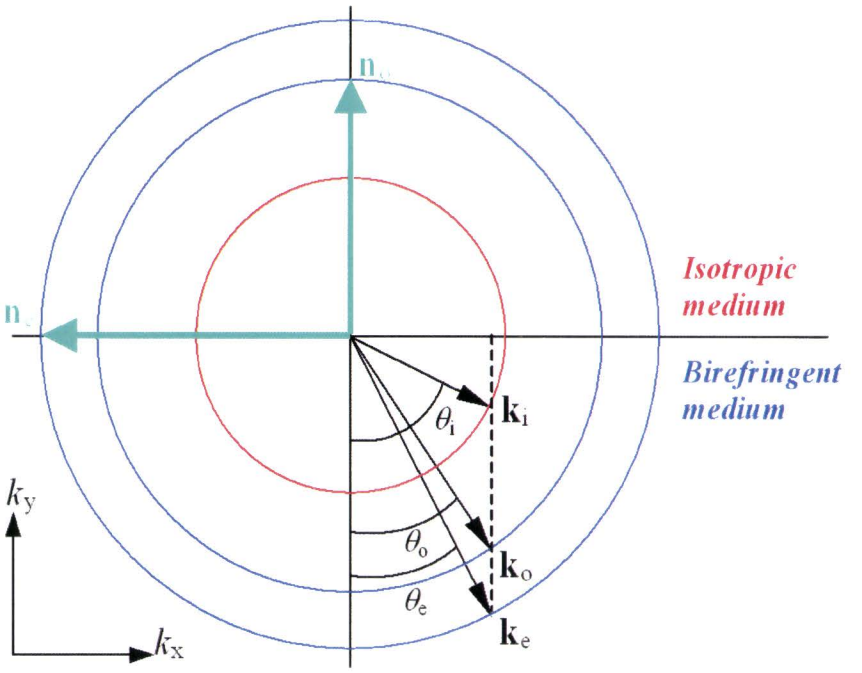

Figure 3.3: Double refraction at a plane birefringent boundary.

Figure 3.3 shows the cross-section of the plane of incidence with the normal surfaces of both media.
The cross-section of the normal surface depicted in red is circular, since the upper medium is optically isotropic. The circle has a radius of curvature n_i.

We first consider the case that the optical axis of the birefringent medium is in the z-direction. As a result, the cross-section of the normal surface consists of two axisymmetric circles, depicted in blue. The inner circle is the normal surface of the ordinary wave with radius of curvature n_o. The outer circle is the normal surface for the extraordinary wave with radius of curvature n_e.

The ordinary wave (with a component of the polarization direction in the xy-plane) and the extraordinary wave (with a component of the polarization direction perpendicular to the polarization direction of the O wave) will be refracted in different directions. This effect is called double refraction.
The incident angle of the incoming wave vector $\mathbf{k}_i$ is θ_i. The angle θ_o is the angle of the refracted ordinary wave vector $\mathbf{k}_o$. The angle θ_e is the angle of the refracted extraordinary wave vector $\mathbf{k}_e$. The boundary condition for the wave vectors requires that

$$k_i \sin\theta_i = k_o \sin\theta_o = k_e \sin\theta_e. \tag{3.25}$$

Equation 3.25 is called Snell's law.

Next, we consider the situation for which the optical axis lies in the plane of incidence. In addition, we assume that the incident light is linearly polarized in

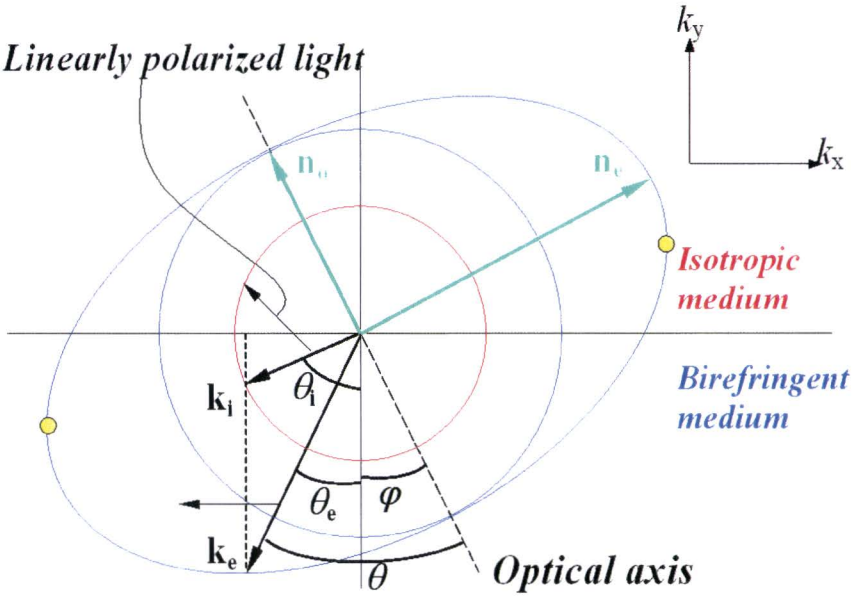

Figure 3.4: Refraction at a boundary of a birefringent medium. Both the optical axis and the direction of polarization lie in the plane of incidence.

the plane of incidence. This situation is depicted in figure 3.4. The birefringent medium has an optical axis under an angle φ with the normal of the boundary. The magnitudes n_o and n_e of the normal surfaces are also indicated.
There is no double refraction, since the linear polarization direction has no z-component. Therefore, according to the theory described in section 3.1, the refracted wave vector can be described by an extraordinary wave. Equation 3.25 reduces to

$$n_i \sin\theta_i = n(\theta) \sin\theta_e, \tag{3.26}$$

where $n(\theta)$ is the index of refraction given by equation 3.20.

The refracted wave vector can be described by an ordinary wave if the polarization direction is in the z-direction. Then, equation 3.25 reduces to

$$n_i \sin\theta_i = n_o \sin\theta_o. \tag{3.27}$$

As a consequence, it is relatively easy to deduce the angle of refraction θ_o.

The case for which $n_i > n_e$ can result in total internal reflection of the incident wave vector. For this situation, the incident angle θ_i equals the angle of refraction.

The angle of refraction θ_e in equation 3.26 can be solved using equation 3.20. This is rather laborious, since n is a function of the angle θ_e.
If we parameterize the sine and cosine in equation 3.26, the terms are transformed to a polynomial function of degree four. This polynomial function has

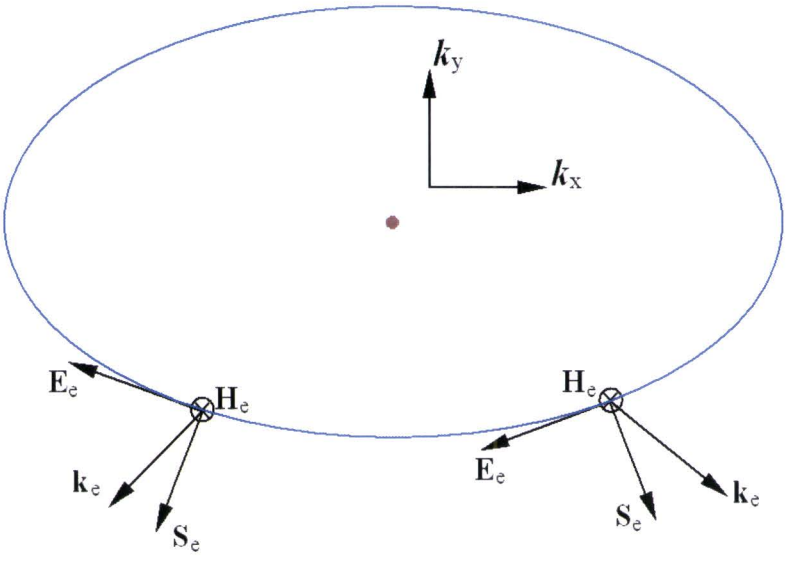

Figure 3.5: The directions of the vectors $\mathbf{k}_e$, $\mathbf{E}_e$, $\mathbf{S}_e$ and $\mathbf{H}_e$ with respect to the normal surface of an extraordinary wave in the principal coordinate system.

four roots, which provide us with four possible angles of refraction. This is not surprising, since we are able to draw four possible wave vectors inside the ellipse for which the magnitude of the tangential components are exactly the same.
A more pragmatic method to determine the angle of refraction θ_e is to solve the problem numerically rather than analytically. This is because the birefringent properties described in this chapter need to be implemented in the tracing program that has already been used in chapter 2. The numerical implementation of these birefringent properties will be discussed in chapter 5.

When using the concept of ray tracing, we are interested in the energy flow of the individual rays. This energy flow is determined by the Poynting vector. The Poynting vector describes the flow of energy per unit area of an electromagnetic wave in terms of electric and magnetic properties. The Poynting vector $\mathbf{S}$ is given by

$$\mathbf{S} = \mathbf{E} \times \mathbf{H}. \tag{3.28}$$

According to equation 3.28, the Poynting vector is always perpendicular to the electric field vector $\mathbf{E}$ and the magnetic field vector $\mathbf{H}$.

For optically isotropic media, the Poynting vector has the same direction as the direction of propagation. This is because the magnetic field vector $\mathbf{H}_o$, the electric field vector $\mathbf{E}_o$ and the direction of propagation $\mathbf{s}$ form an orthogonal triad.
However, for birefringent media, the Poynting vector not necessarily has a direction that is perpendicular to the direction of propagation. This is because the electric field vector $\mathbf{E}_e$ is not perpendicular to the direction of propagation $\mathbf{s}$.

The directions of the relevant vectors of an extraordinary wave with respect to the normal surface are shown in figure 3.5. The electric field vector $\mathbf{E}_e$ is tangent to the normal surface and the Poynting vector $\mathbf{S}_e$ is perpendicular to the normal surface. The wave vector k_e is in line with the center of the ellipse, indicated by the dot. The magnetic field vector H_e is perpendicular to the xy-plane and points away from the reader.

We conclude this theoretical discussion with the following statements. Consider the normal surface in figure 3.4 again. This case involves a refraction of the incident wave vector k_i. The incident wave has a Poynting vector with a negative y-component. It would be in contradiction with the law of conservation of energy if the refracted Poynting vector would have a positive y-component.
In case of refraction, the sign of the y-component of the Poynting vector is conserved. In case of reflection, the sign of the y-component of the Poynting vector is changed.
Consider the case of refraction. If the incident Poynting vector has a negative y-component, only that part of the normal surface for which the refracted Poynting vector has a negative y-component is valid. As a consequence, the part of the normal surface valid for the refracted Poynting vector is limited by the points on the ellipse where the Poynting vector is parallel to the plane boundary (i.e. the points where the derivative of the ellipse is infinite). These points are indicated in figure 3.4, depicted in yellow. The part of the ellipse below these points are accessible for refraction. A similar reasoning applies for the case of reflection.

The main conclusion is that we have all the theory available to be able to trace rays in birefringent media, given the following conditions.
The incident electromagnetic plane wave is linearly polarized and the corresponding polarization direction can be split into two independent modes. In addition, we assumed the wave either to be refracted or reflected. Here, one can discriminate between two situations.
Case 1: The optical axis is perpendicular to the plane of incidence (see figure 3.3). One independent mode is the ordinary wave with a polarization direction perpendicular to the optical axis and index of refraction n_o. The other mode is the extraordinary wave with polarization direction perpendicular to the polarization direction of the ordinary wave with index of refraction given by equation 3.20.
Case 2: The optical axis is in the plane of incidence (see figure 3.4). One mode is the extraordinary wave with polarization direction in the plane of incidence and index of refraction given by equation 3.20. The ordinary wave has a polarization direction perpendicular to the optical axis and index of refraction n_o.

The second case is sufficient for the basic understanding of the birefringent properties of the 2D mode of a switchable lenticular. In order to explain this statement, consider the upper part of figure 3.6. For the investigation of the 2D mode, we assume the optical axis to be in the plane of incidence, i.e. the xz-plane. In addition, by assuming the plane of incidence to be the xz-plane,

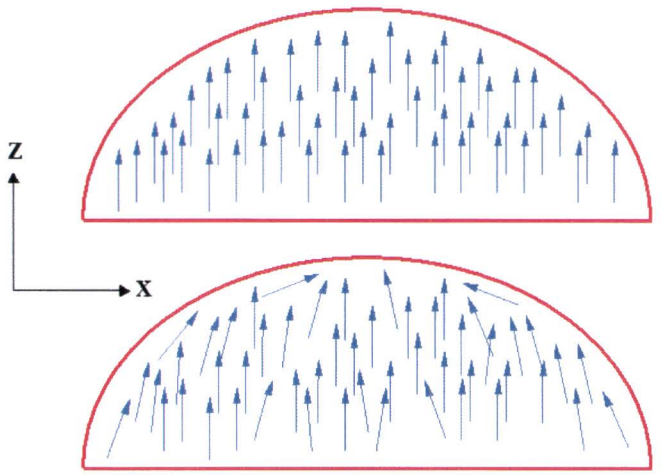

Figure 3.6: The upper part shows a sketch of the LC molecules in a simplified model of the 2D mode of a switchable lenticular. The lower part of the figure shows a sketch of the real situation.

we reduce the birefringent properties of the 2D mode to two dimensions. Note that the orientation of the optical axis is assumed to be independent of the position in the LC material of the lenticular.
In reality, the direction of the director varies throughout the LC material, especially close to the edges of the lens plate, as sketched in the lower part of figure 3.6. The LC molecules have many interactions resulting in different kinds of orientations, better known as twist, bend and splay [10]. In addition, the plane of incidence is not in general in the xz-plane, but can be anywhere in space.
If these effects are taken into account, the optical birefringent properties of the 2D mode become more complicated. Then, other methods are needed for the ray tracing of the 2D mode and 3D mode, for example a finite element method.

4

Analytical model of birefringent 2D mode

Before the 2D mode of a switchable lenticular is submitted to the concept of ray tracing, we investigate the 2D mode analytically. This is done in order to provide us with a qualitative understanding of the birefringent optical properties of a switchable lenticular. How do we expect the qualitative behavior of the 2D mode to be, given the theory of chapter 3?

In this chapter, the 2D mode of a switchable lenticular is analyzed by creating a model that predicts the optical properties of the lenticular under large angles.

For a certain ray, we can discriminate between the propagation of the O wave and the propagation of the E wave. For the O wave, the indices of refraction of the LC and the lens plate do not depend on the viewing angle and remain constant. However, for the E wave, there is a variation in index of refraction, generating a large modulation depth at one particular viewing angle. For this reason, it is the E wave that is investigated in this chapter.

We derive the transfer matrices of a spherical surface and a plane surface under large incident angles. A transfer matrix describes the changes in height and angle of a ray as it makes it way through an optical system.

Using the derived transfer matrices, we deduce the system matrix of a 20 inch switchable 2D/3D display in the 2D mode, applying the birefringent properties described in chapter 3. With this system matrix, we derive the viewing angle under which the focal point of the lenticular is exactly at the pixel structure of the LCD. For this viewing angle, a large modulation depth is generated, since the black matrix is imaged at infinity.

Finally, we introduce the idea of a birefringent lens plate to shift the large modulation depth towards a larger viewing angle. We work out an example and determine the required birefringent properties of the lens plate.

We use the theory in this chapter to investigate the optical properties of a 9 views 20 inch switchable 2D/3D lenticular based display (see also figure 1.10 in chapter 1).

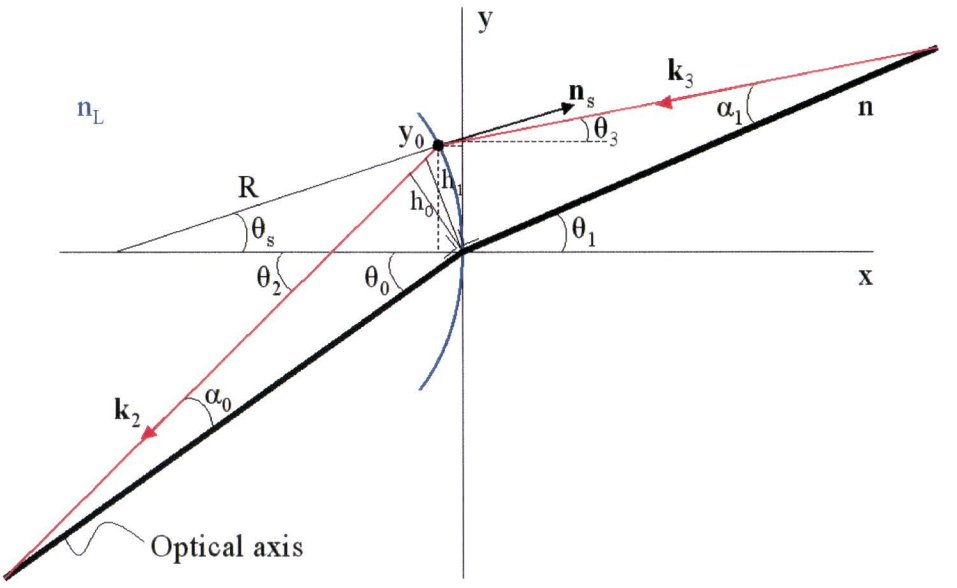

Figure 4.1: Refraction of a paraxial ray at a spherical surface.

4.1 Paraxial model

Consider figure 4.1. The figure shows a spherical surface with radius of curvature R. We define the optical axis of the system by the ray propagating through the origin of the coordinate system. This ray is also known as a finite ray. The medium at the left has an index of refraction n_L and the medium at the right has an index of refraction n.
We investigate a ray (depicted in red) that propagates through the system, having a small deviation from the optical axis. The relations that result from this consideration lead to a 2×2 transfer matrix. The derivation of such a transfer matrix is called a paraxial approximation. A paraxial approximation of a spherical lens can be found in any ordinary book on the subject of geometrical optics [4][5][6]. However, a paraxial approach of a spherical lens under large incident angles is not so standard.

According to figure 4.1, applying Snell's law, a ray propagating exactly along the optical axis is given by

$$n_L \sin\theta_0 = n \sin\theta_1. \tag{4.1}$$

In addition, we apply Snell's law for the ray, depicted in red, at the position indicated by the black dot, at $y = y_0$. In order to do this, we have to parameterize the normal $\mathbf{n}_s$ of the spherical surface, the incident wave vector $\mathbf{k}_3$ and the refracted wave vector $\mathbf{k}_2$. These vectors are given by

$$\mathbf{n}_s = (\cos\theta_s, \sin\theta_s, 0), \tag{4.2}$$

$$\mathbf{k}_2 = |\mathbf{k}_2|(\cos\theta_2, \sin\theta_2, 0) \tag{4.3}$$

and

$$\mathbf{k}_3 = |\mathbf{k}_3|(\cos\theta_3, \sin\theta_3, 0). \tag{4.4}$$

In vector notation, Snell's law is given by

$$\mathbf{n}_s \times \mathbf{k}_2 = \mathbf{n}_s \times \mathbf{k}_3. \tag{4.5}$$

Substituting $\mathbf{k}_3$, $\mathbf{k}_2$ and $\mathbf{n}_s$ in equation 4.5 yields

$$n_L \sin(\theta_2 - \theta_s) = n \sin(\theta_3 - \theta_s). \tag{4.6}$$

This equation can be parameterized and solved for θ_2. We expand the result in a Taylor series around θ_0. Then, the angle θ_2 is given by

$$\theta_2 = \theta_0 + (1 - \frac{n\cos\theta_1}{n_L\cos\theta_0})\theta_s + \frac{n\cos\theta_1}{n_L\cos\theta_0}(\theta_1 - \theta_3), \tag{4.7}$$

ignoring higher order terms.

The transfer matrix is determined by the coordinates (α_0, h_0) and (α_1, h_1) with respect to the optical axis. If $y_0 \ll 1$, the heights h_0 and h_1 are given by $y_0\cos\theta_0$ and $y_0\cos\theta_1$, respectively. With

$$\alpha_0 = \theta_2 - \theta_0 \tag{4.8}$$

and

$$\alpha_1 = \theta_1 - \theta_3, \tag{4.9}$$

we determine the 2×2 transfer matrix $\mathbf{T}$ defined by

$$\begin{pmatrix} y_0\cos\theta_0 \\ \alpha_0 \end{pmatrix} = \mathbf{T} \begin{pmatrix} y_0\cos\theta_1 \\ \alpha_1 \end{pmatrix}, \tag{4.10}$$

with

$$\mathbf{T} = \begin{pmatrix} A & B \\ C & D \end{pmatrix}. \tag{4.11}$$

Using equations 4.7 and 4.10, we can deduce the matrix elements of the transfer matrix $\mathbf{T}$.
Consider the heights h_0 and h_1 at $y = y_0$. In a first order approximation, these heights are linearly related. This implies $h_0 = Ch_1$, with C a constant, independent of the incident angle α_1. If this is the case, $B = 0$ and therefore, $h_0 = Ah_1$. The height h_1 of any paraxial ray is magnified by a factor A, independent of the incident angle α_1. It can be concluded that $B = 0$ and A is given by

$$A = \frac{\cos\theta_0}{\cos\theta_1}. \tag{4.12}$$

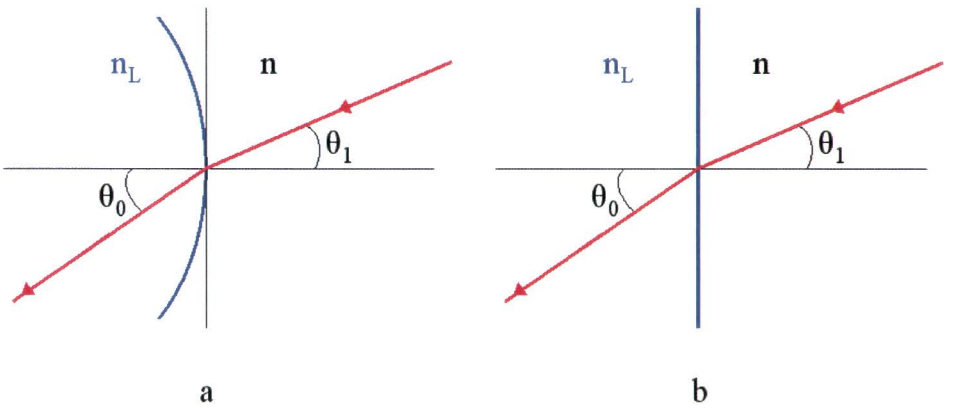

Figure 4.2: Figure a shows the refraction of a ray at a spherical interface, for which the transfer matrix $\mathbf{T}_s$ applies. Figure b shows the refraction of a ray at a plane interface, for which the transfer matrix $\mathbf{T}_p$ applies.

According to equation 4.10, α_1 and α_0 are related by

$$\alpha_0 = Cy_0 \cos\theta_1 + D\alpha_1. \tag{4.13}$$

For $y_0 \ll 1$, the angle θ_s is given by approximately

$$\theta_s \approx \frac{y_0}{R}. \tag{4.14}$$

Then, equation 4.7 is given by

$$\alpha_0 = (1 - \frac{n\cos\theta_1}{n_L\cos\theta_0})\frac{y_0}{R} + \frac{n\cos\theta_1}{n_L\cos\theta_0}\alpha_1 \tag{4.15}$$

From equations 4.13 and 4.15, it can be derived that the remaining elements C and D are given by respectively

$$C = -\frac{1}{R}(\frac{n}{n_L\cos\theta_0} - \frac{1}{\cos\theta_1}) \tag{4.16}$$

and

$$D = \frac{n\cos\theta_1}{n_L\cos\theta_0}. \tag{4.17}$$

Substituting these results in equation 4.11, the transfer matrix $\mathbf{T}_s$ for a spherical surface with radius of curvature R is given by

$$\mathbf{T}_s = \begin{pmatrix} \frac{\cos\theta_0}{\cos\theta_1} & 0 \\ \frac{1}{R}(\frac{n}{n_L\cos\theta_0} - \frac{1}{\cos\theta_1}) & \frac{n\cos\theta_1}{n_L\cos\theta_0} \end{pmatrix}. \tag{4.18}$$

This is the transfer matrix we are looking for.
In the case that θ_0 and θ_1 are both close to zero, $\mathbf{T}_s$ is given by

$$\mathbf{T}_s = \begin{pmatrix} 1 & 0 \\ \frac{1}{R}(\frac{n-n_L}{n_L}) & \frac{n}{n_L} \end{pmatrix} \tag{4.19}$$

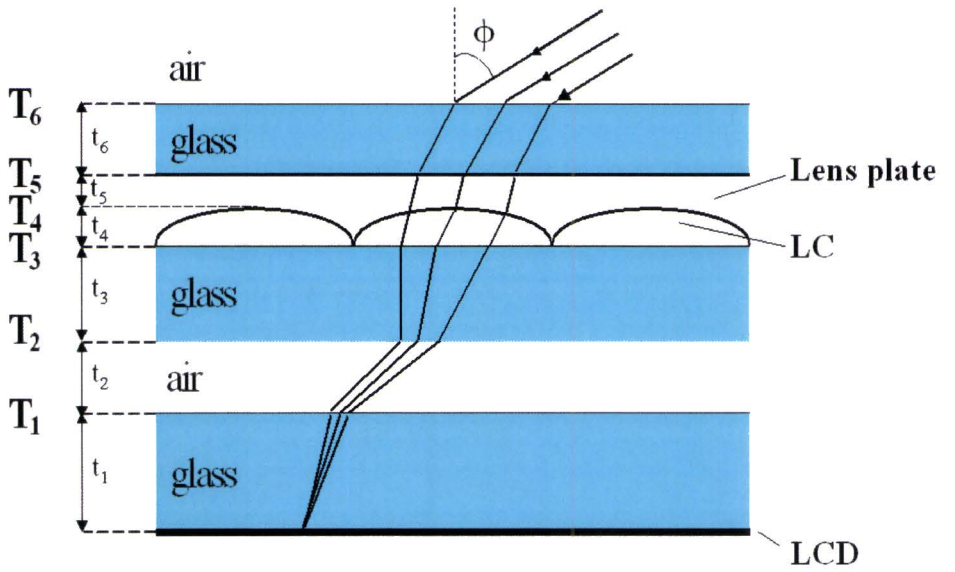

Figure 4.3: Geometry of a 9 views switchable 2D/3D display. For the viewing angel ϕ, the incident parallel rays are exactly focussed at the pixel structure of the LCD.

This is the well-known transfer matrix resulting from a paraxial approximation of a spherical interface, with the x-axis as the optical axis.
If R goes to infinity, we get the transfer matrix $\mathbf{T}_p$ of a plane interface given by

$$\mathbf{T}_p = \begin{pmatrix} \frac{\cos\theta_0}{\cos\theta_1} & 0 \\ 0 & \frac{n\cos\theta_1}{n_L\cos\theta_0} \end{pmatrix} \tag{4.20}$$

The transfer matrix for paraxial translation over a length L is given by

$$\mathbf{T}_L = \begin{pmatrix} 1 & L \\ 0 & 1 \end{pmatrix} \tag{4.21}$$

Figure 4.2a shows the situation where equation 4.18 applies. Figure 4.2b shows the situation where equation 4.20 applies.
With these transfer matrices we can deduce the system matrix of the geometry of a 20 inch switchable 2D/3D display depicted in figure 2.4 in chapter 2.

4.2 Modulation depth in 2D mode

With the derived transfer matrices $\mathbf{T}_s$, $\mathbf{T}_p$ and $\mathbf{T}_L$ we can determine the system matrix $\mathbf{T}_{system}$ of the geometry depicted in figure 4.3. This geometry is the geometry of the 9 views 20 inch switchable 2D/3D display, as defined in section 2.2. The figure shows the relevant thicknesses of the successive layers and defines the relevant transfer matrices.

We define the system matrix as

$$\mathbf{T}_{system} = \mathbf{T}_{t_1}\mathbf{T}_1\mathbf{T}_{t_2}\mathbf{T}_2\mathbf{T}_{t_3}\mathbf{T}_3\mathbf{T}_{t_4}\mathbf{T}_4\mathbf{T}_{t_5}\mathbf{T}_5\mathbf{T}_{t_6}\mathbf{T}_6. \tag{4.22}$$

If the matrix element A of $\mathbf{T}_{system}$ equals zero, the rays depicted in figure 4.3 are entering the system parallel with respect to each other and converge to a point somewhere behind the system. If this point is exactly on the pixel structure of the LCD, such as indicated in figure 4.3, we find the viewing angle ϕ for which the the black matrix is imaged at infinity.

With the help of equations 4.18, 4.20 and 4.21, we can derive a system matrix with matrix element A given by

$$\frac{\cos\theta_6}{\cos\phi} + \left(\frac{t_1}{\cos\theta_1} + \frac{t_2}{\cos\theta_2} + \frac{t_3}{\cos\theta_3}\right)\frac{n_L}{n_g}\frac{\cos\theta_4\cos\theta_6}{\cos\theta_3\cos\phi}\frac{1}{R}\left(\frac{n_{lp}}{n_L\cos\theta_4} - \frac{1}{\cos\theta_3}\right) \tag{4.23}$$

The angles θ_1, ..., θ_6 and ϕ are the angles with respect to the normal of the surfaces 1, ..., 6. The index of refraction n_L of the LC material is given by

$$\frac{1}{n_L^2} = \frac{cos^2\theta_4}{n_o^2} + \frac{sin^2\theta_4}{n_e^2}, \tag{4.24}$$

according to equation 3.20 in section 3.1. The indices n_g and n_{lp} are the indices of refraction of the glass and the lens plate respectively.

We require that $A = 0$. In addition, we use Snell's law at all interfaces. This yields $\theta_1 = \theta_3$, since a glass-air-glass transition involves no changes in the direction of propagation of a ray. These considerations lead to the following equation

$$\frac{t_1}{\cos\theta_1} + \frac{t_2}{\cos\theta_2} + \frac{t_3}{\cos\theta_1} = \frac{n_g\cos\theta_1^2}{n_L\cos\theta_4 - n_{lp}\cos\theta_5}R. \tag{4.25}$$

The right part of equation 4.25 is an expression for the focal distance of the lenticular. The left part in equation 4.25 is exactly the distance for which the focal point is on the pixel structure of the LCD.
Here, we can distinguish between three functions. These are all functions of the angle θ_1 and are given by

$$H_1(\theta_1) = \frac{t_1}{\cos\theta_1} + \frac{t_2}{\cos\theta_2} + \frac{t_3}{\cos\theta_1}, \tag{4.26}$$

$$H_2(\theta_1) = \frac{n_g\cos\theta_1^2}{n_L\cos\theta_4 - n_{lp}\cos\theta_5}R \tag{4.27}$$

and

$$H_3(\theta_1) = \phi(\theta_1) = \arcsin(n_g\sin\theta_1). \tag{4.28}$$

The most efficient way to solve equation 4.25 is by using numerical methods. This can be done by using Newton's method. Newton's method is a root-finding algorithm. We transform this method into a numerical program, written in *c*.

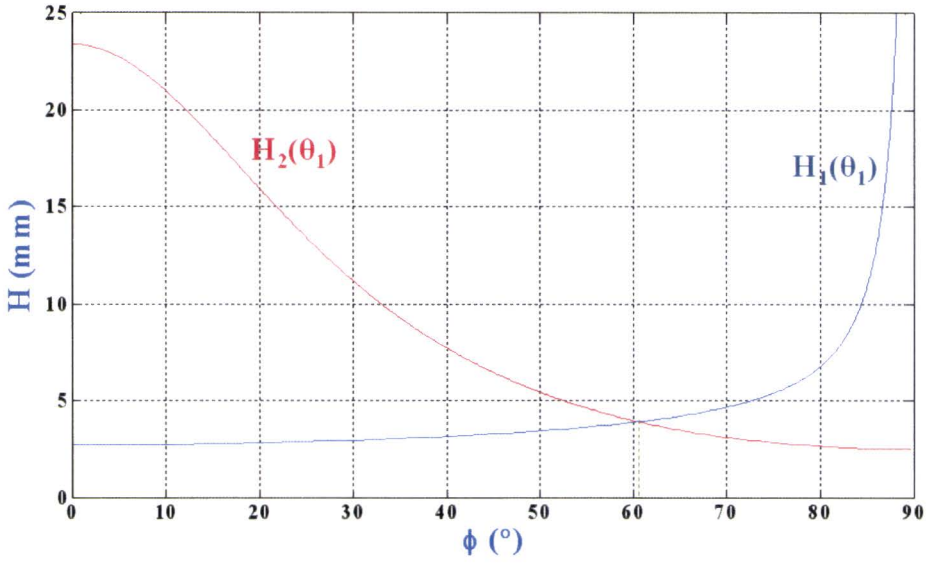

Figure 4.4: The functions H_1 and H_2 as a function of the viewing angle ϕ. The point of intersection indicates the viewing angle for which there exists a large modulation depth. The point of intersection is located at approximately $\phi = 61°$.

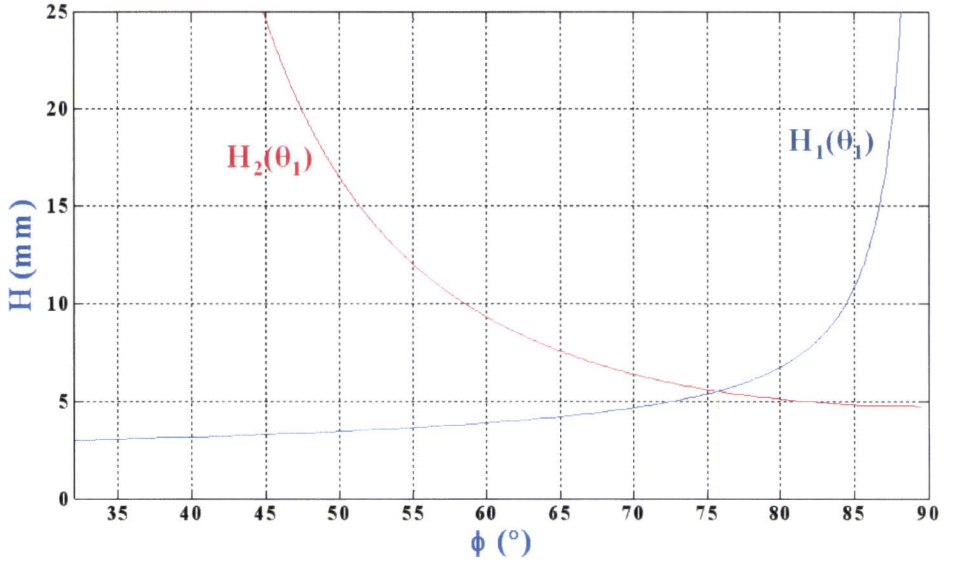

Figure 4.5: H_1 and H_2 as a function of ϕ for $n_{lp} = 1.550$. The point of intersection is located at approximately $\phi = 76°$.

If we take an arbitrary angle θ_1, we can solve the remaining angles, including the viewing angle ϕ, using Snell's law together with Newton's method. Subsequently, we can determine the corresponding functions H_1 and H_2.

By assuming $A = 0$, we also assume a positive lens effect, since the incident parallel rays converge. As a consequence, we have to choose $n_{lp} \leq n_o$. For example, we take $n_{lp} = 1.500$, knowing that $n_o = 1.527$ and $n_e = 1.766$.
Figure 4.4 shows $H_1(\theta_1)$ and $H_2(\theta_1)$ as a function of $\phi(\theta_1)$. We determine the point of intersection of the functions H_1 and H_2. This point of intersection indicates the viewing angle ϕ for which equation 4.25 is valid.
It appears that, according to the paraxial model, a 9 views 20 inch switchable 2D/3D display with $n_{lp} = 1.500$ has a viewing angle of about 61° for which a large modulation depth exists.
Note that these results are true if we consider the birefringent properties of the E wave. The results does not apply for the O wave, since the index of refraction of the O wave is not angular dependent.

In reality, the index of refraction of the lens plate equals 1.550. This means that for small viewing angles, there is a negative lens effect. However, above a certain viewing angle, the effective index of refraction of the lens n_L exceeds the index of refraction of the lens plate n_{lp}. This happens at approximately $\phi = 32°$. For viewing angles above this value, a positive lens effect exists. Figure 4.5 shows the result for $n_{lp} = 1.550$ for viewing angles larger than 32°.
It appears that, according to the paraxial model, a 9 views 20 inch switchable 2D/3D display with $n_{lp} = 1.550$ has a viewing angle of about 76° for which a large modulation depth exists.

We would like to compare the results with observations from a real 20 inch switchable 2D/3D display. When looking at such a display under an angle, we see a mixture of many display effects. In order to test the results which have been derived in this section, we need a well defined and smart experimental setup. With this setup, we investigate the light output of one sub-pixel using polarizers to examine the O wave and the E wave separately. Unfortunately, such an experimental setup is not yet available.

4.3 Birefringent lens plate

We would like to increase the viewing angle for which the black matrix is imaged at infinity towards larger viewing angles. In this section, we suggest a method for which this viewing angle can be transformed to viewing angles over 80°.

Suppose that the lens plate is optically birefringent, having the same birefringent properties as the 2D mode of the switchable lenticular. This is shown in figure 4.6. By changing the $n_{o_{lp}}$ and $n_{e_{lp}}$ of the LC of the lens plate, we change the refractive power of the lens plate. However, we have to be careful choosing the right $n_{o_{lp}}$ and $n_{e_{lp}}$. This is because we would like to change the refractive

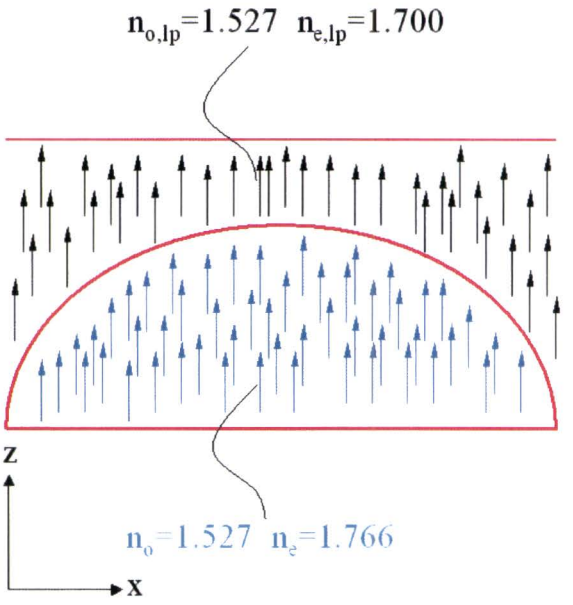

Figure 4.6: Switchable lenticular with optically birefringent lens plate.

power for large viewing angles, keeping optical properties of the lenticular for small viewing angles the same.
Consider equation 3.20 in section 3.1. For small angles θ, n can be approximated by n_o. For larger angles θ, n_e becomes more important. As a consequence, we have to change $n_{e_{lp}}$, keeping $n_{o_{lp}}$ unchanged with respect to the birefringent properties of the switchable lens.

What happens to the 3D performance when changing the refractive power of the lens plate, given the considerations mentioned above?
In the 3D mode, the optical axis of the switchable lens is in the xy-plane and the optical axis of the lens plate is unchanged with respect to the 2D mode, pointing in the z-direction (see figure 4.6).
Light with a polarization direction parallel to the optical axis of the switchable lens in the 3D mode is described by an E wave. It experiences an index of refraction n_e and after refraction an index of refraction $n_{o_{lp}}$ in the birefringent lens plate. As a result, the E wave is transformed to an O wave, with polarization direction perpendicular to the optical axis of the birefringent lens plate. Almost nothing has changed with respect to a non-birefringent lens plate.

For example, we take $n_{o_{lp}} = 1.527$ and $n_{e_{lp}} = 1.700$. The index of refraction n_{lp} is given by

$$\frac{1}{n_{lp}^2} = \frac{cos^2\theta_5}{n_{o_{lp}}^2} + \frac{sin^2\theta_5}{n_{e_{lp}}^2}. \tag{4.29}$$

In this case, there is a perfect index match between n_o and $n_{o_{lp}}$, since for LC material TL213, $n_o = 1.527$. This is desirable, since for $n_o = n_{o_{lp}}$, there are

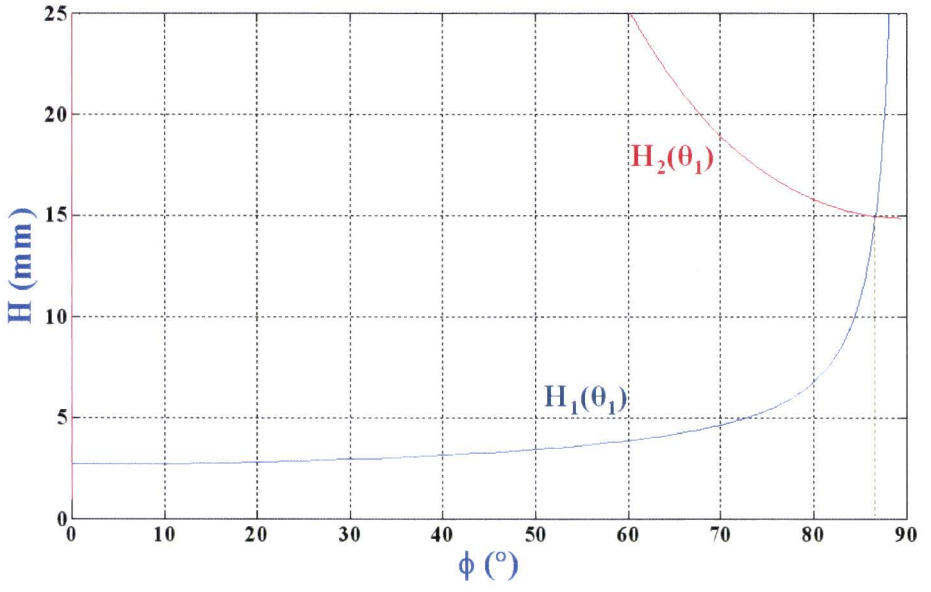

Figure 4.7: The functions H_1 and H_2 as a function of the viewing angle ϕ. This time, the lens plate is also birefringent with $n_{o_{lp}} = 1.527$ and $n_{e_{lp}} = 1.700$. The point of intersection is located at approximately $\phi = 87°$.

no residual lens effects of the switchable lenticular in the 2D mode for small viewing angles for both the O wave and the E wave.
Figure 4.7 shows the results for the defined birefringent lens plate. It can be clearly seen that the viewing angle for which there is a large modulation depth is now approximately 87°.

When $n_o = n_{o_{lp}}$ and $n_e = n_{e_{lp}}$, there is a perfect index match for both the E wave and the O wave. In this case, there are no residual lens effects at all.

It can be concluded that it is possible to increase the viewing angle for which a large modulation depth exists in the 2D mode using a birefringent lens plate. In addition, if we apply a perfect index match between the LC material and the lens plate, there are no substantial residual lens effects. If we assume the lens plate to have the birefringent properties as depicted in figure 4.6, the 3D performance of a switchable 2D/3D display in the 3D mode is not likely to be changed.
In chapter 5, we investigate the large modulation depth in the 2D mode with the help of a ray tracing program.

5

Numerical ray tracing of birefringent 2D mode

In this chapter, we examine the 2D mode of a switchable lenticular using ray tracing. We can not directly use existing ray tracing software, but we have to implement the birefringent properties of the 2D mode. We can do this with the help of the theory described in chapter 3. We construct an algorithm that determines the changes in direction of a ray when refracted or reflected at a birefringent interface.
We use the ray tracing of the 2D mode for a 9 views 20 inch switchable 2D/3D display. We trace the rays that originate from one sub-pixel. From the tracing results, an angular intensity distribution is determined. The angular intensity distributions of the O wave and the E wave are treated separately.
In addition, we trace the design of a 9 views 20 inch switchable 2D/3D display with a birefringent lens plate and compare the results with the theoretical results of chapter 4.

5.1 Birefringent tracing algorithm

In this section, we define a method to determine the changes in direction of a ray when refracted or reflected at a birefringent interface. A method to determine the changes in position are already implemented in the existing ray tracing software.
We define the incident medium as the medium in which an incident ray propagates. The final medium is the medium in which a refracted or reflected ray propagates.

Consider figure 5.1. The figure shows a possible cross-section of the normal surface for an E wave in the incident medium. We define a propagating wave vector $\mathbf{k}$ in a coordinate system (k_x,k_y,k_z). The coordinates are in units of ω/c. The rotation angle φ is the angle under which the optical axis of the incident medium is rotated. Note that the optical axis is in the plane of incidence.
In the principal coordinate system, an ellipse with major axis n_e and minor axis

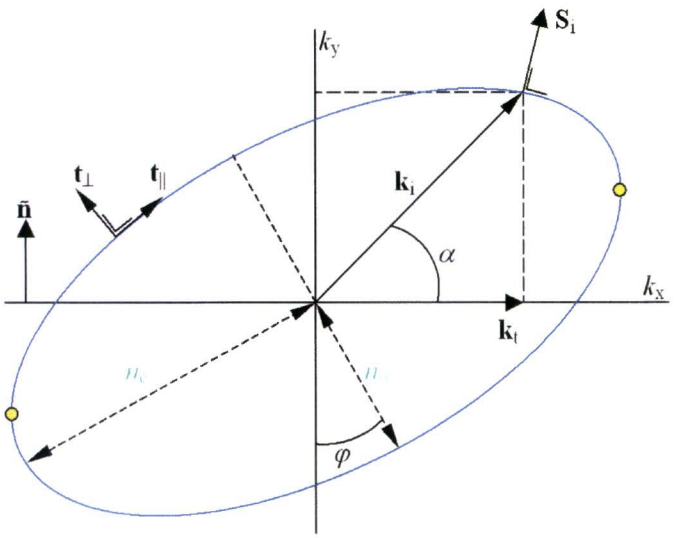

Figure 5.1: Example of a cross-section of the normal surface for an E wave in an incident medium in which an incident wave vector $\mathbf{k}_i$ propagates.

n_o is given by

$$\frac{{n_x}^2}{n_e} + \frac{{n_y}^2}{n_o} = 1. \tag{5.1}$$

The coordinates n_x and n_y can be written as a function of an angle α (conformal mapping), shown in figure 5.1. These coordinates are elliptical coordinates and are given by

$$\begin{pmatrix} n_x \\ n_y \end{pmatrix} = \begin{pmatrix} n_e \cos(\alpha) \\ n_o \sin(\alpha) \end{pmatrix}, \tag{5.2}$$

with

$$0 \leq \alpha < 2\pi. \tag{5.3}$$

The rotation matrix $\Re$ for a positive counterclockwise rotation over an angle φ is given by

$$\Re = \begin{pmatrix} \cos(\varphi) & -\sin(\varphi) \\ \sin(\varphi) & \cos(\varphi) \end{pmatrix}. \tag{5.4}$$

An ellipse rotated under an angle φ can be determined from the product of the rotation matrix with the elliptical coordinates. This yields

$$\Re \begin{pmatrix} n_x \\ n_y \end{pmatrix} = \begin{pmatrix} n_e \cos(\varphi)\cos(\alpha) - n_o \sin(\varphi)\sin(\alpha) \\ n_e \sin(\varphi)\cos(\alpha) + n_o \cos(\varphi)\sin(\alpha) \end{pmatrix}. \tag{5.5}$$

The vector in equation 5.5 corresponds to an incident wave vector $\mathbf{k}_i$, depicted in figure 5.1.

The normal vector and tangent vector of the ellipse can be deduced from equation 5.5. The tangent vector is given by

$$\mathbf{t}_{\parallel} = \frac{\partial}{\partial \alpha} \Re \begin{pmatrix} n_x \\ n_y \end{pmatrix}. \tag{5.6}$$

This yields

$$\mathbf{t}_{\parallel} = \begin{pmatrix} -n_e \cos(\varphi)\sin(\alpha) - n_o \sin(\varphi)\cos(\alpha) \\ -n_e \sin(\varphi)\sin(\alpha) + n_o \cos(\varphi)\cos(\alpha) \end{pmatrix}. \tag{5.7}$$

The normal vector $\mathbf{t}_{\perp}$ is perpendicular to the tangent vector. This yields

$$\mathbf{t}_{\perp} = \begin{pmatrix} \mathbf{t}_{\parallel y} \\ -\mathbf{t}_{\parallel x} \end{pmatrix}. \tag{5.8}$$

We normalize these vectors with a normalization factor given by

$$A = \sqrt{|\mathbf{t}_{\parallel x} \cdot \mathbf{t}_{\parallel y}|}. \tag{5.9}$$

The normalized vectors $\mathbf{t}_{\perp}$ and $\mathbf{t}_{\parallel}$ are depicted in figure 5.1.

Given an arbitrary incident normalized Poynting vector $\mathbf{S}_i$, we have to determine the point of intersection where $\mathbf{S}_i$ is exactly perpendicular to the ellipse. In vector notation, we have to determine the position on the ellipse were

$$\mathbf{S}_i \cdot \mathbf{t}_{\parallel} = 0 \tag{5.10}$$

and

$$\mathbf{S}_i \cdot \mathbf{t}_{\perp} = 1. \tag{5.11}$$

From these conditions, we can deduce the corresponding angle α and the corresponding wave vector $\mathbf{k}_i$, using equation 5.5.

Snell's law says that the tangential component of a refracted or reflected wave vector is conserved. Therefore, we have to determine the tangential component of $\mathbf{k}_i$ along the surface. This vector is given by

$$\mathbf{k}_t = \mathbf{k}_i - (\mathbf{k}_i \cdot \tilde{\mathbf{n}})\tilde{\mathbf{n}}, \tag{5.12}$$

with $\tilde{\mathbf{n}}$ a normalized vector perpendicular to the surface of refraction, depicted in figure 5.1.

Consider figure 5.2. The figure shows the properties of a possible final medium. Again, the optical axis is assumed to be in the plane of incidence.
Given the tangential component $\mathbf{k}_t$ of the incident wave vector, we have to determine a possible refracted or reflected wave vector $\mathbf{k}_r$.
We define the scalar $k_{t,max}$ as the maximum magnitude of the tangential wave vector given the birefringent properties of the final medium. If $|\mathbf{k}_t| \leq k_{t,max}$, the ray is refracted. If $|\mathbf{k}_t| > k_{t,max}$, there are no graphical solutions for $\mathbf{k}_r$ in figure 5.2. Then, the ray is assumed to be reflected.

Consider the case of refraction, depicted in figure 5.2. Given the the wave vector $\mathbf{k}_t$, we have to determine the corresponding angle α in the final medium. This angle is determined by the condition

$$|\mathbf{k}_t|^2 - \mathbf{k}_r \cdot \mathbf{k}_t = 0. \tag{5.13}$$

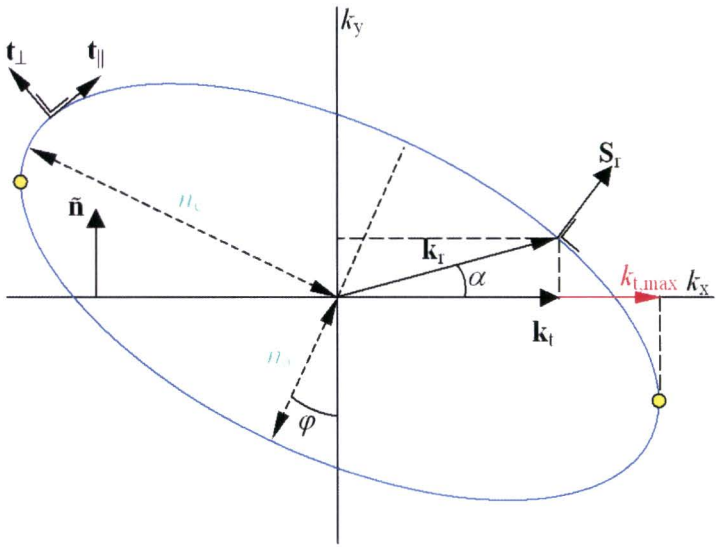

Figure 5.2: Example of the properties of a medium in which a refracted wave vector $\mathbf{k}_r$ propagates.

From this equation, we find two solutions for α. The correct solution for α can be determined using the following condition. For refracted Poynting vectors, the sign of the inner product given by

$$\tilde{\mathbf{n}} \cdot \mathbf{S}_r \tag{5.14}$$

is conserved. In the case of reflection, the sign of this inner product is changed.

With the correct angle α, we determine the corresponding refracted wave vector $\mathbf{k}_r$ using equation 5.5 and the normalized refracted Poynting vector $\mathbf{S}_r$ using equation 5.8.

This method has been translated to c code. The code contains a function whose input is given by the birefringent properties of the incident and final medium, which are the n_o, n_e, the optical axis $\mathbf{c}$, the normal of the surface $\tilde{\mathbf{n}}$ and the incident Poynting vector $\mathbf{S}_i$. The output is the refracted or reflected Poynting vector $\mathbf{S}_r$. The code is given in Appendix A.

The code also contains a function which collects all the relevant information from which an image of the present situation can be formed using Matlab. An example can be seen in figure 5.3. The figure shows an example of refraction. In the upper part of the figure the birefringent properties of an incident medium are depicted including the incident Poynting vector $\mathbf{S}_i$, depicted in yellow. The lower part of the figure shows the properties of the final medium and the refracted Poynting vector $\mathbf{S}_r$. The used parameters are listed below the figure. An example of reflection is given in Appendix B.

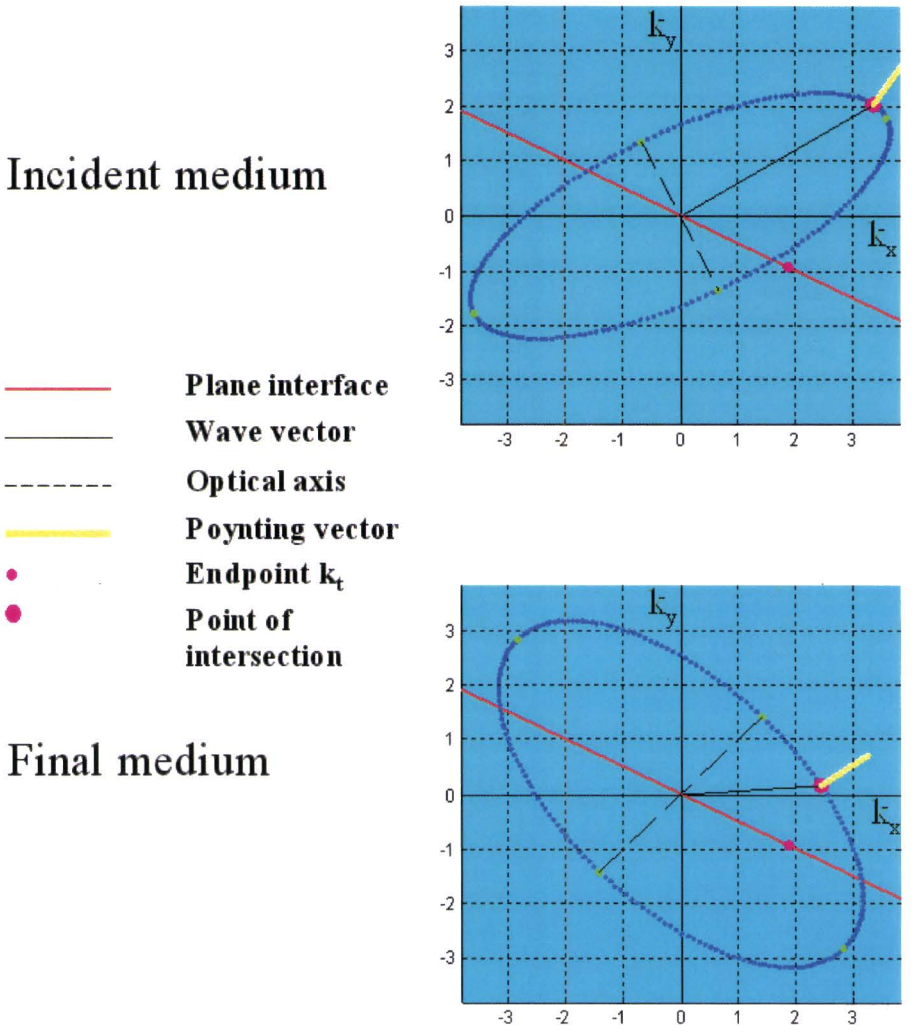

Figure 5.3: Example of refraction, plotted in Matlab. The incident medium is defined by $n_o = 1.500$, $n_e = 4.000$, $\mathbf{c} = (-0.5, 1.0, 0.0)$ and the final medium by $n_o = 2.000$, $n_e = 4.000$, $\mathbf{c} = (1.0, 1.0, 0.0)$. The normal of the interface is given by $\tilde{\mathbf{n}} = (0.5, 1.0, 0.0)$. The incident normalized Poynting vector is $\mathbf{S}_i = (0.55, 0.83, 0.00)$ and the refracted normalized Poynting vector is $\mathbf{S}_r = (0.84, 0.54, 0.0)$.

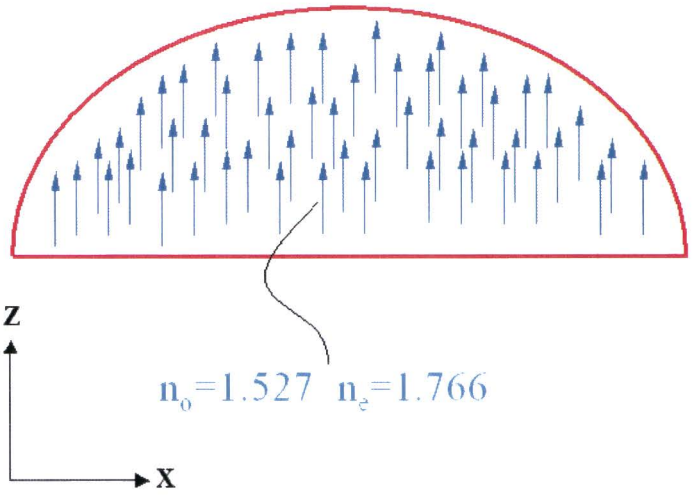

Figure 5.4: Switchable lenticular with orientation of the LC molecules in the z-direction.

With the implementation of this code in the existing ray tracing software, we are able to define birefringent interfaces in the definition of the geometry that is to be traced and calculate the changes in the direction of propagation of individual rays.

5.2 Modulation depth in 2D mode

With the implementation of the tracing algorithm in the existing ray tracing software, it is possible to apply ray tracing for a geometry which contains birefringent interfaces.
For the ray tracing of the 2D mode of a 20 inch switchable 2D/3D display, we use the properties as defined in section 2.2. Figure 5.4 shows the orientations of the LC molecules of the 2D mode of a switchable lenticular. It is assumed that the polarization direction of the light coming from the LCD can be divided in two components. One component is the O wave with polarization direction in the y-direction, having an index of refraction of n_o. The other component is the E wave with polarization direction in the xz-plane, having an index of refraction of n given by equation 3.20. These two components are traced separately.

Figure 5.5 shows the randomly starting positions of a 1000 rays per sub-pixel, indicated by the blue dots. The positions of the dots indicate the defined light-emitting part of a sub-pixel. In between is the black matrix. The black lines indicate the position of a cylindrical lens. It can be seen that the pitch of the lens is approximately 0.38 millimeter, as defined in figure 2.4 in section 2.2. The angle between the sub-pixels and the lenticular equals $\arctan\frac{1}{6}$. In order to verify the correct pixel layout, we compare the sub-pixels of figure 5.5 with

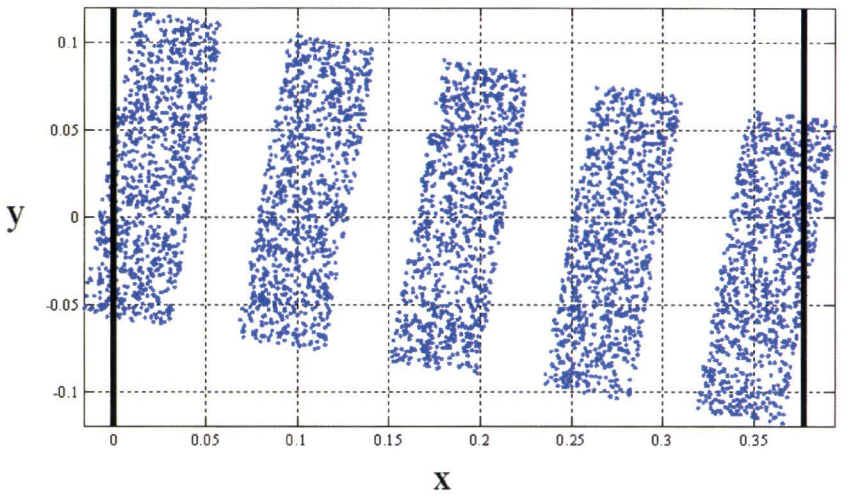

Figure 5.5: Pixel dimensions of a 9 views 20 inch switchable 2D/3D display. The blue dots indicate the starting positions of a 1000 rays per sub-pixel. The area in between the blue dots corresponds to the black matrix.

the sub-pixels numbered by 1, 3, 5, 7 and 9 in figure 1.6 in chapter 1.

In general, we trace 2 million rays per sub-pixel. All these rays are defined in a plane that is perpendicular to the long axis of the lenticular. Subsequently, these rays are projected to the plane defined by $y = 0$. This is done in order to simplify the processing of all data that are produced during the ray tracing.
At a distance above the display, the traced rays are collected in a series of intervals. Each interval of x collects a number of rays. This number of rays is a measure for the intensity of the light coming from the display at this particular interval. All the intervals correspond to a certain viewing angle with respect to the display. As a result, we can determine the angular intensity distribution of a display.

With the tracing program, we trace the light coming from one sub-pixel of a 9 views 20 inch switchable 2D/3D display. The sub-pixel is positioned symmetrically below one of the cylindrical lenses of the lenticular, such as the sub-pixel depicted in figure 5.5 at approximately $x = 0.19$ millimeter. We examine only one sub-pixel, because we want to investigate the qualitative properties of the switchable lenticular in the 2D mode rather than the total intensity distribution resulting from all the sub-pixels of a switchable 2D/3D display.
Figure 5.6 shows the angular intensity distribution of both the O wave (indicated in blue) and the E wave (indicated in red).

For small viewing angles, the intensity distribution of the O wave and the E wave are the same. This is because for small viewing angles, the angle θ between the direction of propagation and the optical axis is small. Then, equation

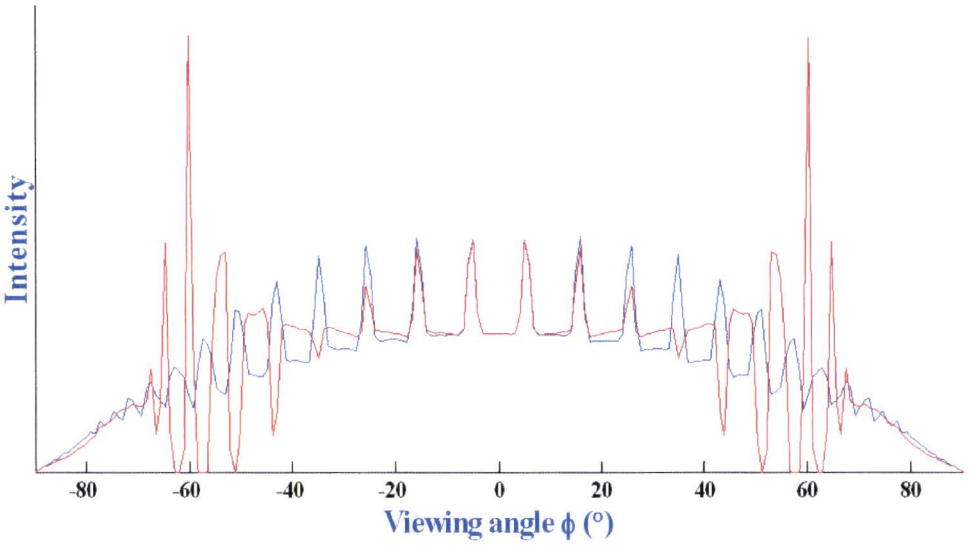

Figure 5.6: Intensity distribution of a 20 inch 9 views switchable 2D/3D display. The blue curve indicates the intensity distribution of the O wave. The red curve indicates the intensity distribution of the E wave.

3.20 reduces to $n = n_o$. This means that both the O wave and the E wave have an index of refraction n_o. As a result, the angular intensity distributions are approximately the same.

For the O wave, there is always a residual negative lens effect, regardless of the viewing angle ϕ. This is because, the index of refraction of the lens plate is 1.550 and the ordinary index of refraction of the LC is 1.527. This residual lens effect can be noticed by the blue peaks in figure 5.6.

For the E wave, there is a negative lens effect for small viewing angles and a positive lens effect for larger viewing angles. Somewhere, there must be a transition from negative to positive lens effect. This transition can be seen in figure 5.6. From the figure, we notice that the red peaks transform to 'grooves' in the intensity distribution. This happens at approximately $\phi = 30°$. This corresponds to the result derived in section 4.2. There, it is found that the index of refraction of the lens n_L exceeds the index of refraction of the lens plate n_{lp} at approximately $\phi = 32°$.

As discussed in chapter 4, there is a viewing angle for which the focal distance is exactly at the pixel structure of the LCD. As a consequence, the black matrix is imaged at infinity.
Figure 5.6 shows that there is a large peak for the E wave at a viewing angle of approximately 60°. Alongside this peak, there is an interval of zero intensity. The interval containing the zero and peak intensities indicates the viewing

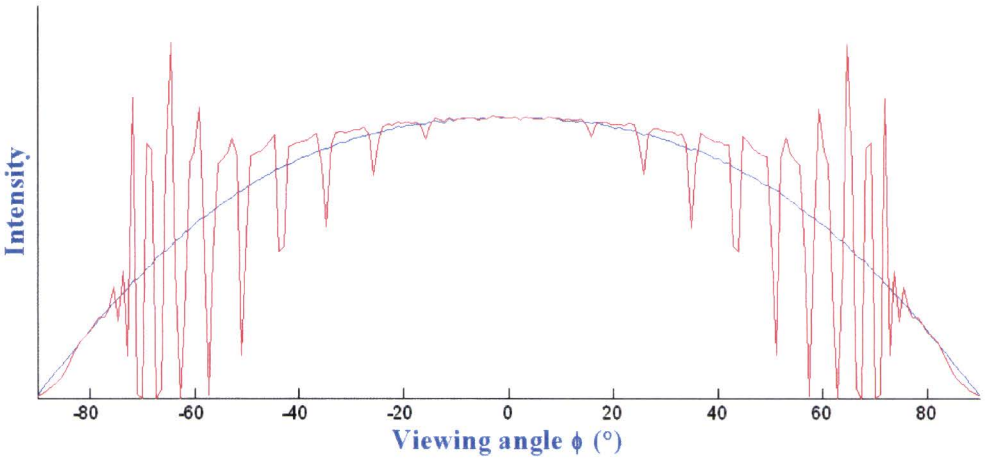

Figure 5.7: Intensity distribution of a 9 views switchable 2D/3D display, with $n_{o_{lp}} = 1.527$ and $n_{e_{lp}} = 1.700$. The blue curve indicates the intensity distribution of the O wave. The red curve indicates the intensity distribution of the E wave.

angles for which the black matrix and the sub-pixels are imaged at infinity. The viewing angle of approximately 60° is not consistent with the theoretical results of section 4.3, which predict a viewing angle of about 76°.

It can be concluded that there is a discrepancy between the theoretical results of chapter 4 and the numerical results presented in this section. Most likely, this is because the paraxial model does not include lens aberrations. This is due to the fact that in the Taylor series, from which equation 4.7 in chapter 4 is deduced, higher order terms are ignored. In contrast to the paraxial model, the numerical results include lens aberrations.
However, the numerical tracing results comply with the qualitative properties of a birefringent switchable lenticular. This gives confidence in the use of the implemented tracing algorithm derived in section 5.1.

5.3 Birefringent lens plate

In this section, we determine the intensity distributions of the O wave and the E wave, coming from one sub-pixel, given that the lens plate is optically birefringent, as defined in section 4.3 (see figure 4.6). The ordinary index of refraction of the lens plate $n_{o_{lp}} = 1.527$ and the extraordinary index of refraction $n_{e_{lp}} = 1.700$. The resulting intensity distribution is depicted in figure 5.7.

For small viewing angles ϕ, $n_{lp} \approx n_L$, since $n_{o_{lp}} = n_o$. This means there is an index match between the lens plate and the LC of the switchable lens. Consequently, there is no residual lens effect for viewing angles close to zero degrees for both the O wave and the E wave, as can be seen in figure 5.7.

The intensity distribution of the O wave has no residual lens effects, since $n_{o_{lp}} = n_o$. This can be seen in figure 5.7, where the blue curve has neither peaks nor grooves.
The E wave, however, shows an increasing positive lens effect for increasing viewing angle ϕ. This is as expected, since the effective index of refraction n_L exceeds the effective index of refraction n_{lp} for any viewing angle ϕ.

Figure 5.7 shows that for approximately 70°, the focal point of the lenticular is at the pixel structure, generating a large modulation depth.

When $n_o = n_{o_{lp}}$ and $n_e = n_{e_{lp}}$, there is a perfect index match for the E wave and the O wave. Then, the red curve in figure 5.7 will transform to the shape of the blue one, resulting in a smooth angular intensity distribution.

We conclude that the theoretical results of section 4.3 do not comply with the numerical tracing results presented in figure 5.7. The reason for this discrepancy is the same as mentioned in section 5.2. Most likely, the discrepancy can be ascribed to the fact that the paraxial model does not include lens aberrations, whereas the numerical results do include lens aberrations.
However, we have been able to increase the viewing angle for which a large modulation depth exists towards larger viewing angles, as can be noticed from figures 5.6 and 5.7.

Based on the findings in this chapter we can draw a very important conclusion. We successfully implemented the developed tracing algorithm of section 5.1, based on the theory we derived in section 3.2, in existing ray tracing software. Subsequently, we have been able to investigate the 2D mode of a switchable lenticular with the help of this tracing program. We achieved this by examining the output intensity distribution of the O wave and the E wave resulting from one sub-pixel. It appears that the tracing results agree with expectations concerning the qualitative behavior of a switchable lenticular in the 2D mode, described in chapter 4.

6

Conclusions

In this thesis, we discuss the concept of multi-view switchable 2D/3D lenticular based displays. We try to improve the 2D and 3D performance by investigating modulation depth and crosstalk. This is done by investigating spherical lenticulars as well as a-spherical lenticulars.

De-focussing of the spherical lenticular can be applied to reduce the modulation depth in the angular intensity distribution of a switchable 2D/3D lenticular based display in the 3D mode.
In order to reduce the modulation depth in the 3D mode even more, the concept of a-spherically shaped lenticulars proves to be an appropriate solution. For a 5 views 2.2 inch switchable 2D/3D display, the modulation depth can be reduced by a factor of two when using an a-spherically shaped lenticular.
It appears that the concept of a-spherically shaped lenticulars is equivalent to an increase in lens aberrations. Consequently, artificially introduced additional lens aberrations can improve the 3D performance of a switchable 2D/3D lenticular based display.
In 2005, Philips Research introduced the concept of fractional views. Here, a shift is introduced in vertical direction between pixels that correspond to one view. With the use of fractional views, the modulation depth of a 4 inch 5 views switchable 2D/3D display can be reduced by two orders of magnitude.

Using Maxwell's equations as a fundamental basis, we developed a theory which describes the refraction and reflection of monochromatic plane waves at plane interfaces between birefringent media. With the help of this theory, we are able to investigate the 2D mode of a switchable lenticular, given a number of conditions. The three-dimensional optical properties of the 2D mode are reduced to two dimensions by assuming the optical axis of the LC material to be in the plane of incidence. Furthermore, we assume the orientation of the optical axis to be position independent, and a plane wave to be either refracted or reflected at a plane interface.

With the use of the developed theory, we investigated the 2D mode of a 20 inch 9 views switchable 2D/3D display analytically. This has been done in order to

provide a better understanding of the qualitative birefringent properties of a switchable lenticular in the 2D mode.
We determined the angular dependency of the modulation depth of the 2D mode. This was achieved by deriving a paraxial model of the lenticular under large viewing angles. With the help of this model, we predicted a viewing angle for which a large modulation depth exists. In order to shift the resulting viewing angle out of the angular viewing zone, we introduced the concept of a birefringent lens plate.
Based on the obtained results, it appears to be feasible to use a birefringent lens plate without disturbing the 3D performance of a switchable 2D/3D display.

In order to use ray tracing to investigate the 2D mode of a 20 inch 9 views switchable 2D/3D display, we developed a tracing algorithm, based on the theory of refraction and reflection of monochromatic plane waves at interfaces between birefringent media. We successfully implemented this tracing algorithm in existing ray tracing software. Subsequently, we have been able to investigate the 2D mode of a switchable lenticular with the help of this tracing program. This was achieved by examining the angular intensity distribution resulting from one sub-pixel.
It appeared that the tracing results agree with the analyzed qualitative behavior of a switchable lenticular in the 2D mode.

It can be concluded that we gained a better understanding on the subject of switchable lenticulars in the 2D mode. Unfortunately, we have not been able to compare the obtained results with a real 20 inch 9 views switchable 2D/3D display. This is because an appropriate experimental setup is not yet available.

Standard ray tracing programs, for instance ASAP or ZEMAX, can trace rays in birefringent geometries only to a certain extent. For example, when there is a gradient in the orientation of the LC molecules, as in GRIN-lenses (graded-index), ray tracing programs show difficulties simulating the birefringent properties.
The ray tracing algorithm developed in this thesis is very well suited to illustrate the behavior of monochromatic plane waves in birefringent media. In the near future, the ray tracing algorithm can be improved and extended to three dimensions. Together with the ray tracing program developed by Philips Research, the ray tracing algorithm can be a useful tool for the simulation of many birefringent geometries.

We conclude this chapter with the following statements. The 3D performance of a switchable 2D/3D lenticular based display in the 3D mode can be improved with the use of artificially introduced additional lens aberrations in a lenticular. The use of this concept can considerably decrease the modulation depth keeping the crosstalk at an acceptable level.
Based on the obtained results, the modulation depth in the 2D mode can be shifted towards larger viewing angles by using the concept of birefringent lens plates. In addition, residual lens effects can be decreased substantially by ap-

plying a perfect index match between the LC material and the lens plate. The concept of birefringent lens plates can be used without disturbing the 3D performance of a switchable 2D/3D display.

Acknowledgement

I would like to thank all people who contributed to this work, in particular:
My supervisor Dr. Ir. Wilbert IJzerman who pointed at switchable 2D/3D displays as a topic for graduation work in the 3D project at Philips Research. His supervision and advise proved to be of great value and this continued to be so when he left the 3D project.
Dr. Dick de Boer, who succeeded Wilbert as a supervisor. From that time, Wilbert and Dick together performed the task of supervisors. I would like to thank them for their efforts and their initiative to point out the possibility of a PhD thesis at Philips Research.
Prof. Dr. Ir. Gerrit Kroesen, my supervisor from the Technical University of Eindhoven, for his visits at Philips Research and his guidance in the realization of this report.
All the people from the groups Visual Experiences and Display Applications and Technologies for nice company.
All the students who accompanied me in room WY 5.43 and WB 3.69: Rob van der Meulen, who provided me with lots of coffee breaks and nice discussions, Sven van Haver, Mathieu Hautefeuille, who accompanied me with many of his friends during the happy hour at the university on Thursday afternoons (also Olivier, who went for a drink during one of the fire drills), Thole Horstman, for his amusing behavior in the corridor, Emanuelle Harel, who decorated the interior with inflatable couches, Xiaosong Ma, for his tofu recipes, Tony, who never drinks coffee, Daan Brinks, with whom I drank a lot of coffee during his programming sessions and finally Leon Kusters, for his funny stories.

Bibliography

[1] S.T. de Zwart, W.L.IJzerman, T. Dekker and W.A.M. Wolter, *A 20" switchable autostereoscopic 2D/3D display*, IDW (2004)

[2] D.F. McAllister, *Stereo Computer Graphics and other True 3D Technologies*, Princeton University Press (1993)

[3] W.L. IJzerman, S.T. de Zwart, T. Dekker, *Switchable 2D/3D displays based on LC-lenses*, TN-2004/00238, Philips Research (2004)

[4] F.L. Pedrotti and L.S. Pedrotti, *Introduction to optics*, second edition, Prentice-Hall International (1996)

[5] E. Hecht, *Optics*, third edition, Addison-Wesley (1998)

[6] M. Born and E. Wolf, *Principles of Optics*, sixth edition, Pergamon Press (1986)

[7] T. Dekker, S.T. de Zwart and W.L. IJzerman, *2D/3D switchable displays*, IMID 2005

[8] S. van Haver, *On the optical design of 3D displays*, TN-2005/00134, Philips Research (2005)

[9] W.L.IJzerman, S.T. de Zwart, T. Dekker, *Design of 2D/3D Switchable Displays*, SID (2005)

[10] P. Yeh and C. Gu, *Optics of Liquid Crystal Displays*, John Wiley & Sons (1999)

[11] J.D. Jackson, *Classical Electrodynamics*, third edition, John Wiley & Sons (1999)

Appendix A

Algorithm code in c

```
#include <iostream.h>
#include "vector.h"
#include "vector.c"

//Author: Maarten Sluijter July 2005

/* Required input: no1, ne1, c-axis1, no2, ne2, c-axis2, S_i, and
n_opp
Output: k_ref, S_ref Note: always choose a positive uniaxial
medium -> ne>no

This program contains six functions:

-birefringe_snellius: applies all functions stated below and
                returns a new Poynting vector S_i
-medium1: calculates tangential wave vector in medium 1
                corresponding to incoming Poynting vector S_i
-refr_refl: calculates maximum tangential wave vector in medium 2
                and compares the result in birefringe_snellius to
                the tangential wave vector of S_i found in medium1
                to determine the case of refraction or reflection
-refract: determines k_ref and S_ref in medium 2 in the case of
                refraction
-reflect: determines k_ref and S_ref in medium 1 in the case of
                reflection
-plot: writes all necessary information to text files that can
                be read in Matlab to create a plot of the
                normal surface and all relevant vectors

The main program defines the input parameters and applies
birefringe_snellius.
*/
```

```
const double pie=3.14159265358979;
const double eps=1e-10;

struct ior
{
    double x;          // ordinary index of refraction
    double y;          // extra-ordinary index of refraction
    vect c;            // c-axis
};

//#define DEBUG_MEDIUM1
int medium1(struct ior *n1, struct vect *S_i, struct vect *n_opp,
            struct vect *k_t, struct vect *k_i)
{
 double alfa_a, alfa_b, alfa_0, phi1;
 double length_k, length_k_t, ctrl, inproduct;
 vect *tauloodrecht;
 tauloodrecht = new vect;

 phi1=-atan2((n1->c).x,(n1->c).z);

 //calculate angle alfa_a where S_i intersects the ellipse
 alfa_a=atan2( (n1->x)*(S_i->z)*cos(phi1) -1.0*(n1->x)*(S_i->x)*sin(phi1),
               (n1->y)*(S_i->x)*cos(phi1) +    (n1->y)*(S_i->z)*sin(phi1) );
 alfa_b=alfa_a+pie;

 //control: inproduct of tauloodrecht with S_i has to be -1
 tauloodrecht->x = -1.0*(n1->y)*sin(phi1)*sin(alfa_a) +
                       (n1->x)*cos(phi1)*cos(alfa_a);
 tauloodrecht->y = 0.0;
 tauloodrecht->z = (n1->y)*cos(phi1)*sin(alfa_a)+(n1->x)*sin(phi1)*cos(alfa_a);

 normalize(tauloodrecht);

 inproduct=inprod(tauloodrecht,S_i);
 ctrl=fabs(inproduct+1.0);

 if (ctrl>eps)
 {
  alfa_a=alfa_b;
 #ifdef DEBUG_MEDIUM1
  tauloodrecht->x = -1.0*(n1->y)*sin(phi1)*sin(alfa_a)+
                        (n1->x)*cos(phi1)*cos(alfa_a);
  tauloodrecht->y = 0.0;
  tauloodrecht->z = (n1->y)*cos(phi1)*sin(alfa_a)+(n1->x)*sin(phi1)*cos(alfa_a)

  normalize(tauloodrecht);
```

```
 inproduct=inprod(tauloodrecht,S_i);
 ctrl=fabs(inproduct+1.0);
 if (ctrl>eps)
 { printf("ERROR! in medium1, inproduct does not equal -1\n"); }
#endif
}

//calculate tangential component k_t
k_i->x= -1.0*(n1->y)*cos(phi1)*cos(alfa_a) +     (n1->x)*sin(phi1)*sin(alfa_a);
k_i->y= 0.0;
k_i->z= -1.0*(n1->y)*sin(phi1)*cos(alfa_a) - 1.0*(n1->x)*cos(phi1)*sin(alfa_a);
//printf("k_i_x:  %18.12f\n",   k_i->x);
//printf("k_i_y:  %18.12f\n",   k_i->y);
//printf("k_i_z:  %18.12f\n\n", k_i->z);

inproduct=-1.0*inprod(k_i,n_opp);
sumprodv(k_i,n_opp,inproduct,k_t);
//printf("k_t_x:  %18.12f\n",   k_t->x);
//printf("k_t_y:  %18.12f\n",   k_t->y);
//printf("k_t_z:  %18.12f\n\n", k_t->z);

//control: k*sin(alfa_0)-k_t=0
length_k=length(k_i);
length_k_t=length(k_t);
alfa_0=acos((-1.0)*inproduct/length_k);
ctrl=length_k*fabs(sin(alfa_0))-length_k_t;
if (ctrl>eps)
{ printf("ERROR! in medium1\n"); }

return(0);
}

int refr_refl(struct ior *n2, struct vect *n_opp, struct vect
*k_tang)
{
double alfa_1, alfa_2, inproduct, ctrl, phi2;
vect *tauevenwijdig; vect *k_1;
tauevenwijdig = new vect; k_1 = new vect;

phi2=-atan2((n2->c).x,(n2->c).z);

//calculate alfa_1 and alfa_2 where tauevenwijdig and n_opp are parallel
alfa_1=atan2(((n2->x)*(n_opp->x)*cos(phi2)+    (n2->x)*(n_opp->z)*sin(phi2)),
             ((n2->y)*(n_opp->x)*sin(phi2)-1.0*(n2->y)*(n_opp->z)*cos(phi2)) );
alfa_2=alfa_1+pie;

//controle: modulus of inproduct of tauevenwijdig with n_opp has to be 1
```

```
 tauevenwijdig->x =-(n2->y)*cos(phi2)*sin(alfa_1)-(n2->x)*sin(phi2)*cos(alfa_1);
 tauevenwijdig->y = 0.0;
 tauevenwijdig->z =-(n2->y)*sin(phi2)*sin(alfa_1)+(n2->x)*cos(phi2)*cos(alfa_1);

 normalize(tauevenwijdig);
 inproduct=inprod(tauevenwijdig,n_opp);
 ctrl=fabs(inproduct)-1.0;

 if (ctrl>eps)
 { printf("ERROR! in refr_refl\n"); }

 //tangential k-vector belonging to angle alfa_1 -> k_tang
 k_1->x = (n2->y)*cos(phi2)*cos(alfa_1) - (n2->x)*sin(phi2)*sin(alfa_1);
 k_1->y = 0.0;
 k_1->z = (n2->y)*sin(phi2)*cos(alfa_1) + (n2->x)*cos(phi2)*sin(alfa_1);
 //printf("k_1_x:  %18.12f\n",   k_1->x);
 //printf("k_1_y:  %18.12f\n",   k_1->y);
 //printf("k_1_z:  %18.12f\n\n", k_1->z);

 inproduct=-1.0*inprod(k_1,n_opp);
 sumprodv(k_1,n_opp,inproduct,k_tang);

 return(0);
}

//#define DEBUG_REFR
int refract(struct ior *n2, struct vect *k_t, struct vect *n_opp,
            struct vect *S_i, struct vect *S_ref, struct vect *k_ref)
{
 int signi, signr;
 double alfa_1, alfa_2, inproduct, ctrl, length_k_t, A, B, C, phi2;

 phi2=-atan2((n2->c).x,(n2->c).z);

 //determine k belonging to k_t in medium 2
 length_k_t=length(k_t);
 A = -1.0*(k_t->x)*(n2->y)*cos(phi2)  -1.0*(k_t->z)*(n2->y)*sin(phi2);
 B = -1.0*(k_t->z)*(n2->x)*cos(phi2)  +    (k_t->x)*(n2->x)*sin(phi2);
 C = length_k_t*length_k_t;
 alfa_1 = 2*atan2((-2*B+sqrt(4*B*B-4*(C-A)*(C+A)))/(2*(C-A)),1.0);
 alfa_2 = 2*atan2((-2*B-sqrt(4*B*B-4*(C-A)*(C+A)))/(2*(C-A)),1.0);

 #ifdef DEBUG_REFR
  printf("alfa_1:  %18.12f\n",   (180/pie)*alfa_1);
  printf("alfa_2:  %18.12f\n",   (180/pie)*alfa_2);
 #endif
```

```
k_ref->x = (n2->y)*cos(phi2)*cos(alfa_1) -1.0*(n2->x)*sin(phi2)*sin(alfa_1);
k_ref->y = 0.0;
k_ref->z = (n2->y)*sin(phi2)*cos(alfa_1) +    (n2->x)*cos(phi2)*sin(alfa_1);

//S_ref=tauloodrecht
S_ref->x = -1.0*(n2->y)*sin(phi2)*sin(alfa_1) + (n2->x)*cos(phi2)*cos(alfa_1);
S_ref->y = 0.0;
S_ref->z = (n2->y)*cos(phi2)*sin(alfa_1)      + (n2->x)*sin(phi2)*cos(alfa_1);

normalize(S_ref);

// |k_t.k_t|-k_ref.k_t=0 & sign of n_opp.S_.. has to be conserved
inproduct=inprod(n_opp,S_i);
if ( inproduct<0.0 ) { signi=-1; } else { signi=1; }
inproduct=inprod(n_opp,S_ref);
if ( inproduct<0.0 ) { signr=-1; } else { signr=1; }
signi=signi*signr;

switch(signi)
{
 case  1: ctrl=inprod(k_ref,k_t); break;
 case -1: alfa_1=alfa_2;
          k_ref->x = (n2->y)*cos(phi2)*cos(alfa_1)
                   - (n2->x)*sin(phi2)*sin(alfa_1);
          k_ref->y = 0.0;
          k_ref->z = (n2->y)*sin(phi2)*cos(alfa_1)
                   + (n2->x)*cos(phi2)*sin(alfa_1);
          S_ref->x = -(n2->y)*sin(phi2)*sin(alfa_1)
                   + (n2->x)*cos(phi2)*cos(alfa_1);
          S_ref->y = 0.0;
          S_ref->z = (n2->y)*cos(phi2)*sin(alfa_1)
                   + (n2->x)*sin(phi2)*cos(alfa_1);
          normalize(S_ref);
          ctrl=inprod(k_ref,k_t); break;
 default: printf("ERROR!!! in refract\n"); break;
}

ctrl=C-ctrl;
if(ctrl>eps)
{ printf("ERROR!!! in refract\n"); }

return(0);
}

int reflect(struct ior *n1, struct vect *k_t, struct vect *n_opp,
            struct vect *S_i, struct vect *S_ref, struct vect *k_ref)
{
```

```
int signi, signr;
double alfa_1, alfa_2, inproduct, ctrl, length_k_t, A, B, C, phi1;

phi1=-atan2((n1->c).x,(n1->c).z);

//determine k belonging to k_t in medium 1
length_k_t=length(k_t);
A=-1.0*(k_t->x)*n1->y*cos(phi1) -1.0* (k_t->z)*n1->y*sin(phi1);
B=-1.0*(k_t->z)*n1->x*cos(phi1) +     (k_t->x)*n1->x*sin(phi1);
C=length_k_t*length_k_t;
alfa_1=2*atan2((-2*B+sqrt(4*B*B-4*(C-A)*(C+A)))/(2*(C-A)),1.0);
alfa_2=2*atan2((-2*B-sqrt(4*B*B-4*(C-A)*(C+A)))/(2*(C-A)),1.0);

#ifdef DEBUG_REFR
 printf("alfa_1:  %18.12f\n",   (180/pie)*alfa_1);
 printf("alfa_2:  %18.12f\n",   (180/pie)*alfa_2);
#endif

k_ref->x = (n1->y)*cos(phi1)*cos(alfa_1) -1.0*(n1->x)*sin(phi1)*sin(alfa_1);
k_ref->y = 0.0;
k_ref->z = (n1->y)*sin(phi1)*cos(alfa_1) +    (n1->x)*cos(phi1)*sin(alfa_1);

//S_ref=tauloodrecht
S_ref->x = -1.0*(n1->y)*sin(phi1)*sin(alfa_1) + (n1->x)*cos(phi1)*cos(alfa_1);
S_ref->y = 0.0;
S_ref->z = (n1->y)*cos(phi1)*sin(alfa_1)      + (n1->x)*sin(phi1)*cos(alfa_1);

normalize(S_ref);

// |k_t.k_t|-k_ref.k_t=0 & sign of n_opp.S_.. has to flip
inproduct=inprod(n_opp,S_i);
if ( inproduct<0.0 ) { signi=-1; } else { signi=1; }
inproduct=inprod(n_opp,S_ref);
if ( inproduct<0.0 ) { signr=-1; } else { signr=1; }
signi=signi*signr;

switch(signi)
{
 case -1: ctrl=inprod(k_ref,k_t); break;
 case  1: alfa_1=alfa_2;
          k_ref->x = (n1->y)*cos(phi1)*cos(alfa_1)
                   - (n1->x)*sin(phi1)*sin(alfa_1);
          k_ref->y = 0.0;
          k_ref->z = (n1->y)*sin(phi1)*cos(alfa_1)
                   + (n1->x)*cos(phi1)*sin(alfa_1);
          S_ref->x = -(n1->y)*sin(phi1)*sin(alfa_1)
                   + (n1->x)*cos(phi1)*cos(alfa_1);
```

```
          S_ref->y = 0.0;
          S_ref->z = (n1->y)*cos(phi1)*sin(alfa_1)
                   + (n1->x)*sin(phi1)*cos(alfa_1);
          normalize(S_ref);
          ctrl=inprod(k_ref,k_t); break;
  default: printf("ERROR!!! in reflect\n"); break;
 }

 ctrl=C-ctrl;
 if(ctrl>eps)
 { printf("ERROR!!! in reflect\n"); }

 return(0);
}

int plot(struct ior *n1, struct ior *n2, struct vect *k, struct
vect *k_t, struct vect *k_ref, struct vect *n_opp, struct vect
*S_i, struct vect *S_ref, int refraction, FILE *fp, FILE *fp2)
//plot ellipse, global coordinate system, plane n_opp, k_i, k_t, k_ref, S_i
//and S_ref for medium 1 and 2 in matlab using ellipsplot.m
{
 double alfa, phi1, phi2;
 int i, j, nalfa=200;

 phi1=-atan2((n1->c).x,(n1->c).z);
 phi2=-atan2((n2->c).x,(n2->c).z);

 vect *n_alfa;
 n_alfa = new vect;

 for(i=0;i<nalfa+1;i++)          //ellipse medium 1
 {
  alfa=i*(pie*2.0)/nalfa;
  fprintf(fp,"%12.10f    ",0.0);
  fprintf(fp,"%12.10f    ",alfa);
  n_alfa->x=(n1->y)*cos(phi1)*cos(alfa) - (n1->x)*sin(phi1)*sin(alfa);
  fprintf(fp,"%12.10f    ",n_alfa->x);
  n_alfa->y=0.0;
  n_alfa->z=(n1->y)*sin(phi1)*cos(alfa) + (n1->x)*cos(phi1)*sin(alfa);
  fprintf(fp,"%12.10f    ",n_alfa->z);
  fprintf(fp,"\n");
 }

 for(j=0;j<nalfa+1;j++)          //ellipse medium 2
 {
  alfa=j*(pie*2.0)/nalfa;
  fprintf(fp2,"%12.10f    ",0.0);
```

```
 fprintf(fp2,"%12.10f    ",alfa);
 n_alfa->x=(n2->y)*cos(phi2)*cos(alfa) - (n2->x)*sin(phi2)*sin(alfa);
 fprintf(fp2,"%12.10f    ",n_alfa->x);
 n_alfa->y=0.0;
 n_alfa->z=(n2->y)*sin(phi2)*cos(alfa) + (n2->x)*cos(phi2)*sin(alfa);
 fprintf(fp2,"%12.10f    ",n_alfa->z);
 fprintf(fp2,"\n");
}

 fprintf(fp,"%12.10f    ",0.0);          fprintf(fp2,"%12.10f    ",0.0);
 fprintf(fp,"%12.10f    ",1.0*(k->y));   fprintf(fp2,"%12.10f    ",0.0);
 fprintf(fp,"%12.10f    ",1.0*(k->x));   fprintf(fp2,"%12.10f    ",0.0);
 fprintf(fp,"%12.10f    ",1.0*(k->z));   fprintf(fp2,"%12.10f    ",0.0);
 fprintf(fp,"\n");                       fprintf(fp2,"\n");

 fprintf(fp,"%12.10f    ",0.0);          fprintf(fp2,"%12.10f    ",0.0);
 fprintf(fp,"%12.10f    ",1.0*(k_t->y));fprintf(fp2,"%12.10f    ",k_t->y);
 fprintf(fp,"%12.10f    ",1.0*(k_t->x));fprintf(fp2,"%12.10f    ",k_t->x);
 fprintf(fp,"%12.10f    ",1.0*(k_t->z));fprintf(fp2,"%12.10f    ",k_t->z);
 fprintf(fp,"\n");                       fprintf(fp2,"\n");

 fprintf(fp,"%12.10f    ",0.0);          fprintf(fp2,"%12.10f    ",0.0);
 fprintf(fp,"%12.10f    ",k_ref->y);     fprintf(fp2,"%12.10f    ",k_ref->y);
 fprintf(fp,"%12.10f    ",k_ref->x);     fprintf(fp2,"%12.10f    ",k_ref->x);
 fprintf(fp,"%12.10f    ",k_ref->z);     fprintf(fp2,"%12.10f    ",k_ref->z);
 fprintf(fp,"\n");                       fprintf(fp2,"\n");

 fprintf(fp,"%12.10f    ",0.0);          fprintf(fp2,"%12.10f    ",0.0);
 fprintf(fp,"%12.10f    ",n_opp->y);     fprintf(fp2,"%12.10f    ",n_opp->y);
 fprintf(fp,"%12.10f    ",-(n_opp->z)); fprintf(fp2,"%12.10f    ",-(n_opp->z));
 fprintf(fp,"%12.10f    ",n_opp->x);     fprintf(fp2,"%12.10f    ",n_opp->x);
 fprintf(fp,"\n");                       fprintf(fp2,"\n");

 fprintf(fp,"%12.10f    ",0.0);          fprintf(fp2,"%12.10f    ",0.0);
 fprintf(fp,"%12.10f    ",S_i->y);       fprintf(fp2,"%12.10f    ",0.0);
 fprintf(fp,"%12.10f    ",S_i->x);       fprintf(fp2,"%12.10f    ",0.0);
 fprintf(fp,"%12.10f    ",S_i->z);       fprintf(fp2,"%12.10f    ",0.0);
 fprintf(fp,"\n");                       fprintf(fp2,"\n");

 fprintf(fp,"%12.10f    ",0.0);          fprintf(fp2,"%12.10f    ",0.0);
 fprintf(fp,"%12.10f    ",S_ref->y);     fprintf(fp2,"%12.10f    ",S_ref->y);
 fprintf(fp,"%12.10f    ",S_ref->x);     fprintf(fp2,"%12.10f    ",S_ref->x);
 fprintf(fp,"%12.10f    ",S_ref->z);     fprintf(fp2,"%12.10f    ",S_ref->z);
 fprintf(fp,"\n");                       fprintf(fp2,"\n");

 fprintf(fp,"%12.10d    ",refraction);  fprintf(fp2,"%12.10d    ",refraction);
 fprintf(fp,"%12.10f    ",n1->x);        fprintf(fp2,"%12.10f    ",n2->x);
```

```
  fprintf(fp,"%12.10f    ",n1->y);        fprintf(fp2,"%12.10f    ",n2->y);
  fprintf(fp,"%12.10f    ",0.0);          fprintf(fp2,"%12.10f    ",0.0);

 return(0);
}

#define DEBUG_BIR_SNEL
int birefringe_snellius(struct vect *n_opp,
struct vect *S_i, struct ior *n1, struct ior *n2, FILE *fp, FILE
*fp2)
{
 int refraction;
 double length_k_tang, length_k_t;
 vect *k_t;    k_t = new vect;
 vect *k;      k = new vect;
 vect *k_tang; k_tang = new vect;
 vect *k_ref;  k_ref = new vect;
 vect *S_ref;  S_ref = new vect;

 normalize(S_i);
 normalize(n_opp);

 //calculate tangential component of incoming wave vector
 medium1(n1, S_i, n_opp, k_t, k);

 #ifdef DEBUG_BIR_SNEL
  printf("k:  %18.12f  %18.12f  %18.12f\n", k->x, k->y, k->z);
  printf("k_t:  %18.12f  %18.12f  %18.12f\n", k_t->x, k_t->y, k_t->z);
  printf("n_opp:  %18.12f  %18.12f  %18.12f\n", n_opp->x, n_opp->y, n_opp->z);
  printf("S_i:  %18.12f  %18.12f  %18.12f\n", S_i->x, S_i->y, S_i->z);
 #endif

 //determine case refraction or reflection
 refr_refl(n2, n_opp, k_tang);
 length_k_tang=length(k_tang);
 length_k_t=length(k_t);

 if (length_k_t<=length_k_tang) { refraction = 1; }
 if (length_k_t>length_k_tang)  { refraction = 0; }

 //calculate refracted/reflected Poynting vector and wave vector
 switch(refraction)
 {
  case 1: printf("refraction:    %1.1d\n\n", refraction);
          refract(n2, k_t, n_opp, S_i, S_ref, k_ref); break;
          //refraction
  case 0: printf("reflection:    %1.1d\n\n", refraction);
```

```
        reflect(n1, k_t, n_opp, S_i, S_ref, k_ref); break;
        //reflection
 default: printf("ERROR! in birefringe_snellius\n"); break;
}

//plot cross section normal surface and Poynting vector for
//medium 1 and 2 in 2 different figures in Matlab using ellipsplot.m

plot(n1, n2, k, k_t, k_ref, n_opp, S_i, S_ref, refraction,  fp, fp2);

#ifdef DEBUG_BIR_SNEL
printf("k_ref_x:  %18.12f\n",   k_ref->x);
printf("k_ref_y:  %18.12f\n",   k_ref->y);
printf("k_ref_z:  %18.12f\n\n", k_ref->z);
printf("S_ref_x:  %18.12f\n",   S_ref->x);
printf("S_ref_y:  %18.12f\n",   S_ref->y);
printf("S_ref_z:  %18.12f\n\n", S_ref->z);
#endif

//copy new direction into old one
copyv(S_ref,S_i);

return(0);
}

void main()
{
FILE *fp; FILE *fp2;
fp=fopen("ellips.txt","w");
fp2=fopen("ellips2.txt","w");

//Input:

//definition medium 1 en 2

 ior *n1;                              ior *n2;
 n1 = new ior;                         n2 = new ior;
 n1->x = 1.5000;                       n2->x = 2.0000;       //no
 n1->y = 4.0000;                       n2->y = 5.0000;       //ne
(n1->c).x = -1.0;                     (n2->c).x = 1.0;       //c-axis
(n1->c).y = 0.0;                      (n2->c).y = 0.0;
(n1->c).z = 1.0;                      (n2->c).z = 1.0;

if (n1->x==n1->y) {(n1->c).z=0.0;(n1->c).x=0.0;}
if (n2->x==n2->y) {(n2->c).z=0.0;(n2->c).x=0.0;}

//define incoming Poynting vector and normal of plane
```

```
 vect *S_i;              vect *n_opp;
 S_i = new vect;         n_opp = new vect;
 S_i->x = -1.000;        n_opp->x = 0.0000;
 S_i->y = 0.0;           n_opp->y = 0.00;
 S_i->z = 0.8800;        n_opp->z = 1.00000;

 //Tracing routine:
 printf("Author: Maarten Sluijter July 2005.\n\n");
 birefringe_snellius(n_opp, S_i, n1, n2, fp, fp2);

 //Output:  S_i (ellipsplot.m)

 fclose(fp);
 fclose(fp2);
 getchar();
}
```

Appendix B

Reflection

In this appendix, an example of reflection at a birefringent interface will be given. In addition, a special case of refraction is examined.

Figure B.1 shows a situation where an incident Poynting vector is reflected. The figure shows a cross-section of the normal surface with the plane of incidence for the incident medium. The incident Poynting vector is depicted in the upper part of the figure and the reflected Poynting vector is depicted in the lower part of the figure. The relevant parameters are listed below the figure. Note that for the reflected Poynting vector, the sign of the inner product given by equation 5.14 in section 5.1 is changed.

Figure B.2 shows a situation where an incident Poynting vector is refracted. The upper part of the figure shows a cross-section of the normal surface with the plane of incidence for the incident medium. The lower part of the figure shows a cross-section of the normal surface with the plane of incidence for the final medium. The incident Poynting vector is depicted in the upper part of the figure and the refracted Poynting vector is depicted in the lower part of the figure. The relevant parameters are listed below the figure.
In this case, the sign of the inner product given by equation 5.14 is conserved, as expected. However, the sign of the x-component of the refracted Poynting vector is changed. This result is rather counter intuitive, since we would expect the sign of the x-component of the refracted Poynting vector to be conserved. However, given the present situation of figure B.2, the result seems perfectly legal.
This situation is merely given to indicate the diversity of situations that can be created using the derived algorithm of section 5.1.

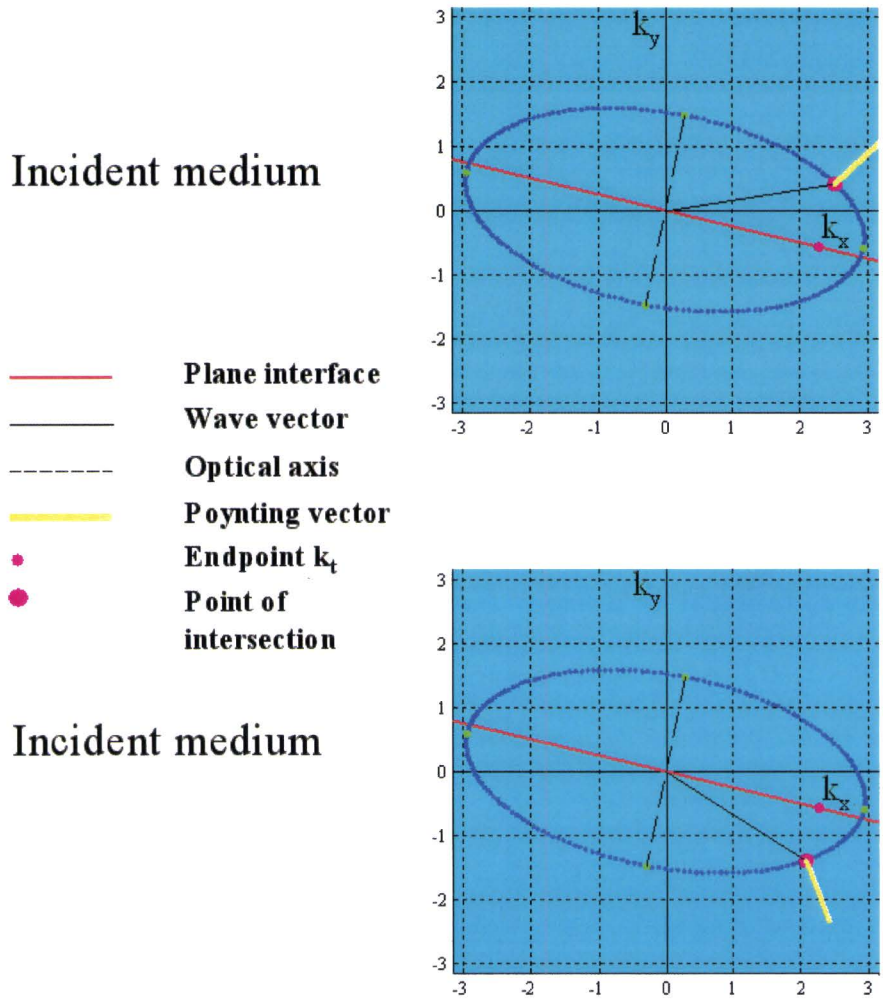

Figure B.1: Example of reflection, plotted in Matlab. The incident medium is defined by $n_o = 1.500$, $n_e = 3.000$, $\mathbf{c} = (0.2, 1.0, 0.0)$ and the final medium by $n_o = 1.000$, $n_e = 1.000$, $\mathbf{c} = (1.0, 1.0, 0.0)$. The normal of the interface is given by $\tilde{\mathbf{n}} = (1.0, 4.0, 0.0)$. The incident normalized Poynting vector is $\mathbf{S}_i = (0.71, 0.71, 0.00)$ and the reflected normalized Poynting vector is $\mathbf{S}_r = (0.34, -0.94, 0.0)$.

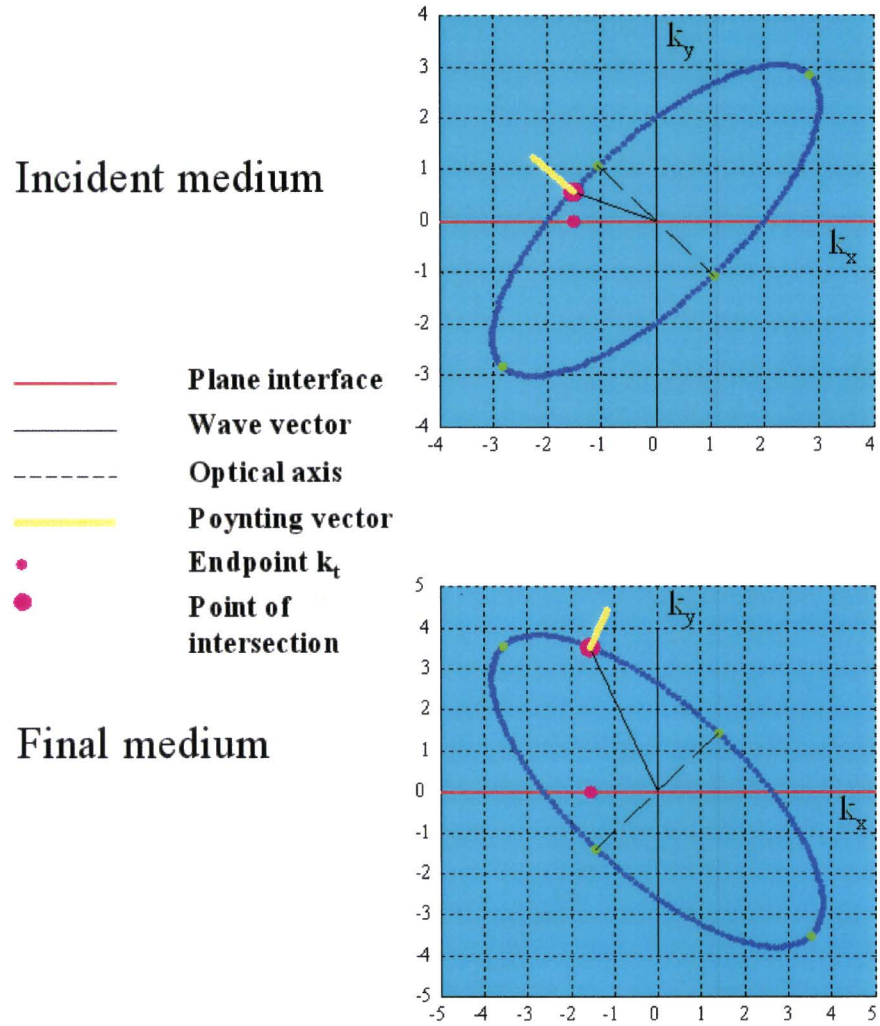

Figure B.2: Example of refraction, plotted in Matlab. The incident medium is defined by $n_o = 1.500$, $n_e = 4.000$, $\mathbf{c} = (-1.0, 1.0, 0.0)$ and the final medium by $n_o = 2.000$, $n_e = 5.000$, $\mathbf{c} = (1.0, 1.0, 0.0)$. The normal of the interface is given by $\tilde{\mathbf{n}} = (0.0, 1.0, 0.0)$. The incident normalized Poynting vector is $\mathbf{S}_i = (-0.75, 0.66, 0.00)$ and the refracted normalized Poynting vector is $\mathbf{S}_r = (0.39, 0.92, 0.0)$.